Mesoscale variability of phosphorus stocks, hydrological and biological processes in the mixed layer in the Eastern Mediterranean Sea in autumn and during an unusually dense winter phytoplankton bloom

France Van Wambeke, Vincent Taillandier, Xavier Durrieu de Madron, Pascal Conan, Mireille Pujo-Pay, Stella Psarra, Sophie Rabouille, Chloé Baumas, Elvira Pulido-Villena

PII: S0967-0637(24)00118-3

DOI: https://doi.org/10.1016/j.dsr.2024.104348

Reference: DSRI 104348

To appear in: *Deep-Sea Research Part I*

Received Date: 11 March 2024

Revised Date: 15 June 2024

Accepted Date: 23 June 2024

Please cite this article as: Van Wambeke, F., Taillandier, V., Durrieu de Madron, X., Conan, P., Pujo-Pay, M., Psarra, S., Rabouille, S., Baumas, C., Pulido-Villena, E., Mesoscale variability of phosphorus stocks, hydrological and biological processes in the mixed layer in the Eastern Mediterranean Sea in autumn and during an unusually dense winter phytoplankton bloom, *Deep-Sea Research Part I*, https://doi.org/10.1016/j.dsr.2024.104348.

Mesoscale variability of phosphorus stocks, hydrological and biological processes in the mixed layer in the Eastern Mediterranean Sea in autumn and during an unusually dense winter phytoplankton bloom.

France Van Wambeke[1*], Vincent Taillandier[2], Xavier Durrieu de Madron[3], Pascal Conan[4,5], Mireille Pujo-Pay[4], Stella Psarra[6], Sophie Rabouille[4], Chloé Baumas[1,7], Elvira Pulido-Villena[1]

[1]Aix-Marseille Université, Université de Toulon, CNRS, IRD, Mediterranean Institute of Oceanography (MIO), Marseille, France
[2] Sorbonne Université, CNRS, Laboratoire d'Océanographie de Villefranche (LOV), Villefranche-sur-Mer, France
[3] Université de Perpignan Via Domitia, CNRS – UMR 5110, Centre d'Etude et de Formation sur les Environnements Méditerranéens (CEFREM), 66100, Perpignan, France
[4] Sorbonne Université, CNRS – UMR7621, Laboratoire d'Océanographie Microbienne (LOMIC), Observatoire Océanologique, 66650, Banyuls/mer, France
[5] Sorbonne Université, CNRS OSU STAMAR - UAR2017, 4 Place Jussieu, 75252 Paris cedex 05, France
[6] Hellenic Centre for Marine Research (HCMR) Institute of Oceanography, 71003, Crete, Greece
[7] present address: Earth System Science, Stanford University, Stanford, CA, United States

***corresponding author** france.van-wambeke@mio.osupytheas.fr

Highlights

- Significant role of mixing episodes in winter in eastern Mediterranean Sea
- meso-scale variability in the mixed layer (P-depleted) affects P cycle and populations
- Phosphomonoesterase and phosphodiesterase kinetics tracers of P availability
- An important, winter phytoplankton bloom evidenced in the vicinity of the Rhodes gyre
- Highest cell specific phosphatases were seen in the Rhodes gyre

Abstract

We investigated spatiotemporal variations of nutrients, dissolved organic pools (C, N, P), phosphomonoesterase (PME) and phosphodiesterase (PDE) activities, heterotrophic prokaryotic production and planktonic microorganisms within the mixed layer (ML) in the Eastern Mediterranean Sea. We characterized two contrasted situations: autumn 2018 (highly stratified period, deep chlorophyll maximum within 100 m depth) and winter 2019 (including a bloom period). We compared the distribution of biogeochemical variables within the mixed layer and hydrological vertical structure between the different stations using a principal component analysis. Six groups of stations were identified (one group in autumn, 5 in winter), based on variable physical descriptors but also environmental biogeochemical conditions related to i) the seasonal aspect (for instance, all stations sampled within the Ierapetra anticyclone in autumn clustered in one, single group); ii) transitions between cyclonic and anticyclonic structures with a large range of ML depths (18-269 m) and indications of intense, preceding winter convection events: iii) progression of a high phytoplankton bloom during the winter cruise inferred from a series of observations: a strong nitrate drawdown, important growth of *Synechococcus*, pico and nano eukaryotes, accumulation of

chlorophyll a (> 60 mg m^{-2}), primary production rates up to 509 mg C m^{-2} d^{-1}, changes in the pigments' diversity, increase in biomass-specific ectoenzymatic activities and of heterotrophic prokaryotic production, all in conjunction with the vicinity of the Rhodes gyre. Here, we studied the distribution of biological and biogeochemical properties within the mixed layer, in particular by employing sensitive methods for the detection of low phosphate concentrations and of the labile dissolved organic phosphorus pool. From this data set, we demonstrate that the surface mixed layer classically considered as a P-depleted and uniform layer in the Eastern Mediterranean Sea was highly biologically dynamic, and prone to rapid spatio-temporal changes in phosphatase activities and phytoplankton dynamics. Altogether, these data reveal a strong short-term population dynamics. The results highlight the role of mixing episodes in winter, which provide pulsed supplies of phosphate and /or nitrate from the deeper layer to the euphotic zone, triggering transient blooms that often go undetected by satellites.

Keywords:
Eastern Mediterranean Sea
P-depleted
Mixed layer
mesoscale
phosphomonoesterase
phosphodiesterase
organic phosphorus
primary production

1. Introduction

The Eastern Mediterranean Sea (EMS) is one of the most oligotrophic oceanic areas (Reich et al., 2022). Based on satellite imagery analysis (D'Ortenzio and Ribera d'Alcalà, 2009) it is described as a non-blooming region, a situation attributed to a rather shallow mixing reaching only ~ 200 m depth and a resulting in a low supply of nutrients in late winter-early spring (D'Ortenzio et al., 2005; Mayot et al. 2016). The ultra-oligotrophic character of the EMS is partly due to the circulation of Levantine Intermediate Waters (LIW), which acts as a kind of 'conveyor belt' exporting organic matter from the Eastern to the Western Basin (Crise et al., 1999; Pujo-Pay et al., 2011; Moutin and Prieur, 2012; Krom et al., 2014). According to Powley et al. (2017), the main source of P and N in the Mediterranean Sea is the North Atlantic Water entering through the strait

of Gibraltar and propagating to the east. With DIP concentrations < 20 nM during most of the year, the EMS is then particularly impoverished in P relative to N, leading to high N:P molar ratios in epipelagic waters, and even in deep layers (Durrieu de Madron et al., 2011; Pujo-Pay et al., 2011; Powley et al., 2017).

Despite the ultra-oligotrophic character of the EMS, phytoplankton growth is intermittently and sparsely pulsed by mesoscale activity (Krom et al., 1992; Moran et al., 2001; Moutin and Prieur, 2012, Varkitzi et al., 2020; Belkin et al., 2022). In the Levantine Sea, for instance, winter mixing within the cyclonic Rhodes gyre allows the establishment of a recurrent spring bloom in this area (Yilmaz and Tugrul, 1998; D'Ortenzio et al., 2021; Taillandier et al., 2022). The intensity of the bloom within the Rhodes gyre depends on the vertical extent of the previous winter mixing and is highly variable through the years (D'Ortenzio and Ribera d'Alcalà, 2009; Mayot et al., 2016; Habib et al., 2023).

Other intermittent blooms have also been detected in some areas of the EMS, like in the Cretan Sea. For instance, Varkitzi et al. (2020), for instance, observed an exceptional phytoplankton bloom in spring 2008, triggered by the nutrient enrichment that followed a deep mixing event consequent to a cyclonic formation and a preceding strong convection. Indeed, cyclonic formation is known to shoal the nutriclines, thereby stimulating phytoplankton production, net community production, as well as respiration and bacterial production, in comparison to adjacent areas or anticyclonic areas (Sweeney et al., 2003; Maixandeau et al., 2005; Mouriño-Carballido and McGillicuddy, 2006). The EMS also presents a series of cyclones and anticyclones (Barboni et al., 2023).

The availability of nutrients for primary production in the sunlit layer is modulated by the depths of the nitracline and phosphacline as well as the diffusive fluxes across these interfaces. In the Mediterranean Sea, the difference between the depths of the nitracline (usually shallower) and phosphacline (usually deeper) are maximal in late summer, ranging from 100 m (Pujo-Pay et al., 2011) to 600 m (Ediger and Yilmaz, 1996) in the Levantine Basin and ranging from 300 to 400 m in the southeastern Ionian Sea (Klein et al., 2003). The consequence is that concentrations of dissolved inorganic phosphorus (DIP) within the surface, mixed layer (ML) are typically close to the detection limits of standard analytical techniques employing the molybdenum blue reaction (Djaoudi et al., 2018b). In contrast, nitrate (NO_3^-) is re-supplied in surface layers after winter convection events, when these are strong enough to reach the nitracline (Ben Ezra et al., 2021). The mixed layer depth (MLD) varies seasonally, under the influence of mesoscale structures and deep convection events followed by re-stratification episodes (D'Ortenzio et al., 2005; Taillandier et al., 2022; Barboni et al., 2023). The ML also receives external fluxes of N and P, both in mineral and organic forms, from atmospheric deposition (Pullido-Villena et al., 2021). Intermittent atmospheric

deposition events, for example Saharan dust events, could rapidly modify biogeochemical fluxes and activities within it (Van Wambeke et al., 2021).

Considering how deep nutriclines usually are in the EMS, the mixed layer remains isolated from the nutriclines most of the year. The low nutrient availability combined with a shallow mixed layer (ML) lead to the formation of a nutrient-depleted layer extending below the ML. However, the quantification of nanomolar variations of DIP allowed revealing diffusive (Pullido-Villena et al., 2021) and advection fluxes (Van Wambeke et al., 2021) between the nutrient-depleted layer and the ML. Under the influence of such intermittent fluxes, the planktonic microorganisms in the ML face variable degrees of limitation and may present different type of responses, for example the production of ectoenzymes (Hoppe, 1983). Among others, one form of adaptation facing P-limitation is the utilization of exogenous P-monoesters and P-diesters through the production of phosphomonoesterase (PME) and phosphodiesterase (PDE). Both types of enzymes are expressed by some species of phytoplankton and heterotrophic prokaryotes (Dunlap and Callahan, 1993; Yamaguchi et al., 2014; Luo et al., 2009; Noskova et al., 2019; Huang et al., 2021). PME has frequently been determined in different oceanic provinces (Su et al., 2023) and is often used as an index of P-deficiency in Mediterranean Sea (Sala et al., 2001; Van Wambeke et al., 2002, Zaccone et al., 2012; Céa et al., 2014) due to the negative correlation generally observed between DIP concentration and PME activity. The possibility to detect nanomolar concentration of DIP (Zhang and Chi, 2002) allowed assessing chemical fractions of dissolved organic phosphorous (DOP) like the phosphomonoesters and phosphodiesters (Yamaguchi et al., 2019). In parallel, the use of artificial phosphodiester's substrates allowed assessing PDE activities by colorimetry of fluorimetry (Sato et al., 2013; Thomson et al., 2020; Van Wambeke et al., 2023).

We propose here an analysis of the biogeochemical and biological variability within the ML in the eastern Mediterranean around Crete, with a particular focus on the P cycle. We considered two distinct seasons: autumn (October), chosen to represent typically warm, stratified and intense oligotrophic conditions, and late winter (February-March), chosen to illustrate the period associated to episodic phytoplankton growth. We characterized the distribution of nutrients, dissolved organic phosphorus (DOP) and its labile fraction (L_{DOP}), as well as both types of phosphatase activities (PME and PDE) in the ML, associated with the circulation features and microbial populations present, in these two contrasted seasonal situations.

2. Materials and Methods

2.1. Sampling

An extensive investigation of the western Levantine Sea (Eastern Mediterranean) was carried out in the framework of the French program MISTRALS-Mermex project and its component PERLE

(Pelagic Ecosystem Response to dense water formation in the Levant Experiment, D'Ortenzio et al., 2021). This study focuses on 2 cruises conducted in 11-20 October 2018 (PERLE1) and 27 February-15 March 2019 (PERLE2). PERLE1 cruise, on board the R/V 'l'Atalante', targeted the region around Ierapetra anticyclone located south-east of Crete (Fig. 1). During PERLE2 cruise, on board the R/V 'Pourquoi Pas?', the area sampled was extended all around Crete, including Kassos and Karpathos Straits on the eastern side, and Antikithira Strait on the western side (Fig. 2). For both cruises, oceanographic stations were carried out using a CTD-rosette equipped with a sampling system of 24 Niskin bottles and a Sea-Bird SBE9plus underwater unit equipped with pressure, temperature, conductivity, oxygen and chlorophyll fluorescence sensors. Stations numbers used in this study were identified by the number of the CTD cast.

Water sub-samples from the Niskin bottles were taken for quantification of biogenic elements (inorganic and organic C, N, P, including nanomolar analyses of DIP and L_{DOP}), flow cytometry counts, pigment concentrations), heterotrophic prokaryotic production (BP) and phosphatase activity (PME and PDE activities). At each station, selected depths were sampled: 10 depths for BP, DIP and L_{DOP} (between 0 and 200 m during PERLE1 and 0 and 300 m during PERLE2), and among these, 6 for PME and PDE activities. Other nutrient analyses (nitrate, nitrite, dissolved organic phosphorus, DIP with the classical method) were sampled more intensively, at 12 depths between surface and 300 m depth. Primary production (PP) was measured only at a few selected stations (see below).

2.2. Nutrients

Seawater samples for standard nutrient analysis were filtered online (0.45µm cellulose acetate filters) directly from the Niskin bottles in 20 ml acid-washed polyethylene vials and were stored frozen until analysis in the laboratory for PERLE1, while immediately analyzed on board for PERLE2. Samples were collected in acid-washed polyethylene bottles. Nutrient concentrations of silicate, nitrate, nitrite, and phosphate were determined by colorimetry (Aminot and Kérouel, 2007) using a segmented flow analyzer Seal-Bran-Luebbe (AAIII HR SealAnalytical©) with analytical precision of 0.05 µM, 0.02 µM, 0.01 µM and 0.01 µM, respectively. Detection limits were 0.01 µM for nitrate + nitrite (NOx) and 0.01 µM for phosphate (DIP). Ammonium concentrations (analytical precision ± 2 nM) were determined on board for PERLE1 and PERLE2 by nanomolar fluorometric method (Holmes et al., 1999) on a fluorometer Jasco FP-2020. Samples for the determination of nanomolar concentrations of DIP were collected in HDPE bottles previously cleaned with supra-pure HCl after filtration through 0.2 µm. During PERLE1, samples were stored frozen until analysis in the laboratory. During PERLE2, samples were analyzed on board immediately after sampling.

Nanomolar DIP was analyzed using the liquid waveguide capillary cell (LWCC) method after Zhang and Chi (2002), with a detection limit of 1 nM. Ultrapure water was both used as blank and wash solution in between samples, with a wash time/sampling time of 120s/120s. Because the reagents are pumped through the system continuously, blank signals from the reagents are set to zero during analysis. To test for the refractive index offset due to the difference in salinity between ultrapure wash water and seawater sample, seawater samples were run again at the end of the analytical run without the ascorbic acid reagent. The absorbance of this refractive index offset was subtracted from the sample absorbance before calculating the final phosphate concentration. Total dissolved phosphorus (TDP) and nitrogen (TDN) were measured using the segmented flow analyzer technique after high-temperature (120 °C) persulfate wet oxidation mineralization (Pujo-Pay and Raimbault, 1994; Pujo-Pay et al., 1997). Dissolved organic phosphorus (DOP) was obtained as the difference between TDP and DIP and dissolved organic nitrogen (DON) as the difference between TDN and the sum (NOx + ammonium). The monoesterase hydrolysable fraction of DOP (L_{DOP}) was estimated after enzymatic hydrolysis of the < 0.2 µm filtrate in the presence of a purified phosphatase alkaline (AP) enzyme from *Escherichia Coli* (Sigma P4252) (Djaoudi et al., 2018a) in HDPE bottles. The AP was diluted with pure water to prepare a working solution of 0.2 U mL^{-1}. Equal volumes (0.6 mL) of AP working solution and Tris buffer (0.5 M, pH 8) were added to 30 mL of the < 0.2 µm filtered samples. Samples were then incubated during 3 h in the dark at 30°C. The duration of the incubation and the hydrolysis efficiency was checked with glucose 6-phosphate. After incubation, samples were stored frozen until analysis (PERLE1) or analyzed onboard (PERLE2). L_{DOP} was obtained as the difference in DIP concentration before and after incubation. A blank was run at each station consisting on 30 mL ultrapure water in which 0.6 mL of working AP solution and Tris buffer were introduced. Samples for DOC concentration were filtered through two precombusted (24 h, 450 C) glass fiber filters (Whatman GF/F, 25 mm) and collected in precombusted glass ampoules and acidified to pH < 2 with phosphoric acid. Ampoules were immediately sealed and stored in the dark until analyses by high-temperature catalytic oxidation (HTCO) on a Shimadzu TOC-L analyzer (Cauwet, 1999). The system was calibrated daily with a solution of acetanilide. Typical analytical precision is 0.1 - 0.5 µM (sd) or 0.2–0.5% (CV).

2.3. Biological stocks and fluxes in the epipelagic waters

Flow cytometry was used for the enumeration of small phytoplankton, and heterotrophic prokaryotes (Hprok) using standard techniques (Marie et al., 1997, Marie et al., 2000) described in detail in Van Wambeke et al. (2023). Phytoplankton were classified in different groups according to their distributions in 2 scatter plots of red fluorescence vs side scatter and red fluorescence vs orange fluorescence (Marie et al., 2000): *Prochlorococcus* (Proc), *Synechococcus* (Syn),

picophytoeukaryotes (Picoeuk), nanophytoeukaryotes (Nanoeuk) and Cryptophytes-like cells (Crypto).

Algal pigments markers were analyzed as in Ras et al. (2008). The volume filtered through GF/F filters was 2.8 L per sample and a fine resolution of pigments was only possible in the winter situation We quantified chlorophyll a (chla), divinyl-chlorophyll a (dv-chla), peridinin (peri), fucoxanthin (fuco), alloxanthin (allo), zeaxanthin (zea), 19' butanoyloxyfucoxanthin (19'BF), 19' hexanoyloxyfucoxanthin (19'HF), chlorophyll b (chlb), pheophorbid a and pheophytin a. In autumn, concentrations of some of these pigments were not available, as peri or dv-chla for instance, or phaeopigments. In this study, pigments were available only at selected stations: (ST15, 21, 35, 44, 50, 58, 75, 80, 90, 94, 111 and 116 in winter, and ST2, 5, 12 16, 20 23 and 27 in October). Total chlorophyll a (Tchla) is the sum of chla and dv-chla. The pigment degradation index was calculated as (pheophytin a + pheophorbid a): Tchla ratio. The total phytoplankton biomass expressed in carbon mass (phyto-C) was estimated using the measured Tchla and assuming an overall C:Tchla ratio of 33 on winter and 70 in autumn, taken as an average value cited for ML layers in the Mediterranean Sea (Bellacicco et al., 2016). Heterotrophic prokaryotic biomass (hprok-C) was derived from the cytometry counts, assuming 10 fgC per cell.

During PERLE1 cruise, primary production was estimated by the ^{13}C:^{15}N dual isotopic method (Raimbault and Garcia., 2008) at the same geographic positions corresponding to the CTD casts 2, 15, 25 and 27 but sampled sometimes on another cast (3, 14, 25 and 27, respectively) at sunrise the same day; however only the ^{13}C data are exploited here. At 4 depths (5, 10, 20, 50 m), water samples were collected in triplicate into acid-leached 500 ml polycarbonate bottles just before the sunrise. All bottles filled to the top (final volume 600 ml) were enriched with 0.5 ml of a $NaH^{13}CO_3$ solution (24 g L^{-1}, 99.2 % 13C, EURISOTOP) for C fixation. Bottles were incubated for 24 h (from sun rise to sunrise) under simulated *in situ* conditions and sea surface temperature, in 4 flow-through tanks covered with light blue screens simulating irradiance at each corresponding depth. At the end of the incubation, each bottle was filtered directly onto 25 mm Whatmann GF/F pre-combusted glass fiber filters for the ^{13}C treatment. All filters were then stored at 60°C for the duration of the cruise and stored in a dry place until mass spectrometry analysis within 2 months. The isotopic enrichment and particulate organic carbon analyses were performed using an Integra-CN mass spectrometer. Before analysis, the filters were acidified with 100 µL H_2SO_4 (0.5N) to remove inorganic matter.

During PERLE2 cruise, primary production was estimated by the ^{14}C technique of Steemann-Nielsen (1952). Sea water was sampled from 6 depths (5, 10, 20, 50, 75, 100 m) along the euphotic

zone at the stations 15, 35, 75, 83, 90 and 116. Samples were distributed in 250 ml polycarbonate bottles (2 light and 1 dark for each depth) and water (310 ml in the full bottle) were spiked with 25 µCi of $NaH^{14}CO_3$ (Perkin-Elmer, specific activity 50.8 Ci $mmol^{-1}$). The bottles were incubated under the same conditions as used during PERLE1 cruise (24h-long, on deck incubators, blue screens). After incubation, the samples were immediately filtered onto 0.2, 0.6 and 2 µm pore-size polycarbonate filters (Millipore). Filters were soaked in 1 ml 0.1 N HCl and allowed to stand in uncapped 20 ml vials in order to remove excess ^{14}C-bicarbonate, for approximately 24 h, before 10 ml scintillation cocktail (Ultimagold MV) was added. Counting was performed on a Packard Liquid Scintillation Counter. Disintegrations per minute (dpm) from filters incubated in dark conditions were subtracted from the respective light ones. We used a value of 26400 mg C m^{-3} for the concentration of dissolved inorganic carbon (Pujo-Pay et al., 2011) and a value of 1.05 for the isotopic discrimination factor.

To determine heterotrophic prokaryotic production (BP), samples were incubated with tritiated leucine using the microcentrifuge technique (Smith and Azam, 1992) in the dark in temperature-controlled incubators as detailed in Van Wambeke et al. (2021). We used the empirical conversion factor of 1.5 ng C per pmol of incorporated leucine according to Kirchman (1993). Isotope dilution was negligible under these saturating concentrations as periodically checked with concentration kinetics. BP was measured only during PERLE2 cruise.

Ectoenzymatic activities were measured fluorometrically, using the fluorogenic model substrates 4-methylumbelliferyl-phosphate (MUF-P, Sigma) and bis(4-methylumbelliferyl) phosphate (bisMUF-P, Chem. Pex) to assess phosphomonoesterase (PME) and phosphodiesterase (PDE) activities, respectively. The release of MUF from fluorogenic substrates was followed by measuring the increase in fluorescence in the dark (excitation/emission 365/450 nm, wavelength bandwidth 5 nm) using a VARIOSCAN LUX microplate reader. Between each measurement, the plates were incubated in a temperature-controlled incubator set at the *in situ* temperature, in the dark. Final concentrations used in the 2 ml wells ranged from 0.025 to 1 µM for MUF-P, and 0.025 to 50 µM for bis-MUF-P. Indeed, PDE saturated around 50 µM whereas PME saturated around 1 µM (Van Wambeke et al., 2023). The parameters Vm (maximum hydrolysis rate) and Km (Michaelis-Menten half-saturation concentration that reflects enzyme affinity for the substrate) as well as their corresponding standard errors were estimated by non-linear regression (PRISM) using the Michaelis-Menten equation:

$$V = Vm \cdot \frac{S}{Km + S}$$

where V is the hydrolysis rate and S the fluorogenic substrate concentration added. Turnovertimes (TT) were calculated as the Km:Vm ratio.

285

2.4. Data processing and diagnostics

Measurements by CTD sensors were processed into 1-m resolution vertical profiles for *in-situ* temperature (temp), salinity (SAL), potential density anomaly referenced to surface (i.e. common term sigma-theta, here after designed as 'density', abbreviated σ). In vivo fluorescence measured
290 with the fluorescence sensor mounted on the rosette was calibrated by Tchla concentration. Several diagnostics were implemented on this dataset in order to provide a hydrodynamical context for each station and assess a set of physical properties: the depth of isopycnal 29.05 kg m^{-3} (PISO) and the dynamic topography (in dyn m) relative to 500 dbar (H500) were computed to relocate every station within mesoscale features. The mixed layer depth (MLD) was also estimated at every station to
295 characterize the extent and physical content of surface layers. Using density profiles, MLD was computed as the depth where the residual mass content (i.e., the vertical integral of the density anomaly relative to the surface) reached 1 kg m^{-2} (Prieur et al., 2020). More details on this processing and diagnostics are given in the section 'data and methods' of Taillandier et al. (2022). The methodology used to determine phosphacline and nitracline depths (ZPCline and ZNCline,
300 respectively), as well as DIP and NOx gradients across isopycnals ($\partial DIP/\partial\sigma$ and $\partial NOx/\partial\sigma$, respectively) are detailed in the supplementary section.

For this study focusing on the dynamics within the mixed layers, we selected only the volumetric data sampled inside the mixed layer for each variable of interest: (temp, SAL, σ, nutrients (NOx, DIP, $L_{DOP,}$ DOP, DON, DOC), biological stocks (flow cytometric counts of Hprok, Proc, Syn, Pico-
305 euk, Nano-euk, Crypto-like cells and phyto-C), pigments, and ectoenzymatic activities (Vm and Km values of PME and PDE) and BP inside ML for each station. We also computed selected combinations of variables such as the biomass specific Vm PME and PDE, or NOx:DIP molar ratio. Finally, some variables allowing to characterize each vertical profile (MLD, PISO, H500, ZNcline, ZPcline, $\partial DIP/\partial\sigma$ and $\partial NOx/\partial\sigma$ were also used to link biogeochemical properties with the
310 hydrological structure as derived from the respective CTD cast. A principal component analysis (PCA) was run using stations as observations and physical and biogeochemical parameters as variables. We observed a temporal change in the biogeochemical variables in the epipelagic zone as the phytoplankton bloom evolved during the winter cruise. Including both biological and hydrological variables in the PCA allowed considering both drivers in the system dynamics. All
315 data were normalized before analysis. ST16 (PERLE 1 cruise) as well as ST58 (PERLE2 cruise) were excluded from the PCA analysis since the corresponding data set was incomplete. BP was also

excluded from PCA analysis as it was only available during PERLE2 cruise, as well as PP that was determined only at few stations of both cruises. In summary, the PCA was run with 27 observations and 31 variables in an initial run. Then, we restricted the number of variables to 22 to remove auto-correlations (see results), and added the 9 remaining variables as supplementary descriptive variables, as a compromise between their independency (reducing autocorrelations), their projection on the PCA axes and their contribution to the variance (Fig. 3).

The distributions of medians inside groups determined from the PCA results are presented using box-plots on Figures 4 to 7, S5 and Tables S1 and S2; statistical difference between groups was tested by a bilateral Kruskal-Wallis test; if one group at least was different from any other at $p < 0.05$, then multiple paired comparisons between groups were run using Dunn test.

3. Results

3.1 Overview: mesoscale distribution and biogeochemical vertical patterns.

The dynamic topography (Figs. 1 and 2) for both cruises evidenced intense mesoscale activity in the study region. In the autumn cruise (PERLE1), during which essentially Ierapetra anticyclonic gyre was sampled, vertical profiles of density, Tchla and DIP were more or less similar at all stations (Fig S3a, b, c). Sea surface temperatures ranged from 26.5 to 27.8 °C, with a substantial thermal stratification. The mean MLD (35 ± 19 m, Table 1) was significantly shallower than in winter (83 ± 69 m, Mann Whitney test, $p = 0.012$) and the Pcline was deeper than the Ncline. Concentration gradients across isopycnals at the nutriclines were on average $\partial DIP/\partial\sigma$: 1000 ± 150 µmol kg^{-1} and $\partial NOx/\partial\sigma$: 16 ± 2 mmol kg^{-1}. Nanomolar phosphate data revealed increasing phosphate concentrations with depth from the surface to the upper bond of the P-cline (i.e. inside the P-depleted layer) at 5 stations. At these stations a secondary DIP gradient across isopycnals was thus detectable within the P-depleted layer (i.e. linear regression ∂DIP *vs* $\partial\sigma$ significant at $p < 0.05$) only at 5 in autumn and 4 stations in winter (Table S3). A deep chlorophyll maximum (DCM) was detectable around 100 m depth during the autumn cruise (Fig. S3a). During the winter cruise (PERLE2), the sea surface temperature ranged from 15.5 to 17.4 °C. The deepest MLD were observed in the Cretan Sea (ST1, 13, 15, Fig. 4a, Fig. S4g) and in the center of Ierapetra anticyclone which moved south of Crete between the 2 cruises (ST50, Fig. S3d). At these stations, vertical distribution of chlorophyll was more homogeneous and reached deeper layers accordingly (Fig S4g). In contrast, some stations sampled along the easternmost transect (e.g. ST80 and 94) were located in extensions at the periphery of the Rhodes gyre and presented shallower MLD and 29.05 isopycnal depths (Table 1, Fig. S4d). Pcline and Ncline depths showed a great variability during the winter cruise (ZPcline: 15 m to 265 m, ZNcline: 0 m to 240 m) and some of the data were associated to large uncertainties. For some stations, the ZNcline was unexpectedly shallower than

the ML (Table 1). For instance, at the ST1 (Fig. S2) mean NOx concentrations within the ML were 0.99 µM, and considering only the depth intercept at 0 NOx concentration clearly underestimated that of ZNcline. If we had considered the depth intercept at 0.99 µM NOx concentration, the ZNcline would have resulted to be much deeper (190 m). For 11 stations in winter, high and homogeneous concentrations of NOx in the ML (> 0.4 µM) were obtained, raising the limits of the methodology used here to compute ZNcline. For those we calculated both types of depth intercepts and their associated errors (data not shown). The ZPcline was, like in autumn, and whatever the methodology used, in most cases equal or deeper than the ZNcline, considering the errors of measurements that were sometimes high (Table 1). Concentration gradients across isopycnals were on average $\partial DIP/\partial\sigma$: 1862 ± 988 µmol kg^{-1} and $\partial NOx/\partial\sigma$: 38 ± 16 mmol kg^{-1}, both being most gradual at ST50, 104 and 108 situated in anticyclonic areas, and the steepest at ST116 (Table S3). Both gradients were, on average, significantly higher in the winter cruise (Mann-Whiney test, $p < 0.05$). Nanomolar gradients of DIP concentration across isopycnals inside the P-depleted layer were detectable in 4 stations (Table S3).

Integrated DIP, NOx, L_{DOP} and DOP stocks (0-200 m) were lower in autumn than in winter, and DOP stocks largely exceeded those of DIP during both cruises (Table 2). Integrated Tchla stocks ranged from 11 to 23 mg Tchla m^{-2} during the autumn cruise and from 28 to 69 mg Tchla m^{-2} during the winter cruise. Integrated heterotrophic bacterial production, not sampled during the autumn cruise, ranged from 19 to 77 mg C m^{-2} d^{-1} during the winter cruise (Table 2). Integrated primary production ranged from 39 to 123 mg C m^{-2} d^{-1} in autumn and from 360 to 509 mg C m^{-2} d^{-1} in winter (Table 3). During both cruises, PP peaked within the surface or subsurface layers according to the stations and decreased with depth, except at ST75, where PP values were uniform between surface and 100 m depth (Fig S5). In autumn, maximum rates per unit volume varied between 1.4 and 2.7 mg C m^{-3} day^{-1} (Fig S6) and they were much higher in winter, varying between 4.5 and 12 mg C m^{-3} day^{-1}. PP significantly correlated with Tchla during the winter cruise (log-log linear regression, $p < 0.0001$; $r = 0.67$, $n = 36$), but not in autumn (log-log regression, $n = 16$, $p > 0.05$). BP, measured only during the winter cruise, significantly correlated with PP (log-log regression, $p < 0.0001$; $r = 0.64$, $n = 35$).

The study of PDE and PME kinetics over the whole epipelagic layer is the focus of a companion paper (Van Wambeke et al., 2024), in which we showed that although PME saturated after addition of 1 µM MUF-P, PDE only saturated after adding 50 µM addition of bis-MUF-P. Hence Km and turnover times are much higher for PDE than for PME, as shown also within the ML (Table S2). Vm PME ranged from 0.01 to 18.9 nmol P hydrolyzed L^{-1} h^{-1} and Vm PDE ranged from 0.01 to 23.4 nmol P hydrolyzed L^{-1} h^{-1}, decreasing along the water column (Fig. S3c, f, i, Fig. S4c, f, i). The lowest surface and subsurface Vm PME and PDE were reached at ST1, 13, 15. The highest value of

Vm PME was reached at ST80, 5 m and that of Vm PDE at ST90, 5 m, so that all the extremes were encountered during the winter cruise. The vertical variability of maximum rates (Vm) and of the half saturation constants (Km) of the kinetics of both enzymes is presented and discussed in detail in Van Wambeke et al. (2023). Briefly, both Vm PDE and Vm PME tended to increase when DIP concentration decreased, and activities were particularly triggered when DIP was lower than 10-15 nM. The Vm PME:Vm PDE ratio was close to 1 (mean ± sd: 1.10 ± 0.98) and increased when DIP concentration decreased.

3.2. Station clustering

Stations from both cruises discriminated in clusters on the biplot of the first two axes obtained in the PCA (Fig. 3). The first two principal components (PC1 and PC2) together explained 63% of the total variance. We observed 6 groups visually distinct. All of PERLE1 (autumn cruise) stations were into one, clearly distinct group (A). Group A was characterized by thin ML (Fig 4a), higher dynamic heights (Fig. 4b) and greater depths of isopycnal 29.05 kg m^{-3} (Fig. 4c), reflecting the season (autumn) and the dynamical properties of an anticyclone such as Ierapetra, on which the cruise PERLE1 particularly focused. This was consistent with higher temperature and salinity inside the ML, as shown by addition of these supplementary variables (Table S1, Fig. 3, Fig. 4d). The stations of the winter cruise (PERLE2) were distributed in five distinct groups (B to F). Groups B, D and E rather partitioned according to the physical properties of the water column (anticyclone vs cyclone), while group F assembled stations based on the trends of biogeochemical variables inside the ML. The difference between groups D and E resulted also mainly from differences in the biogeochemical variables within the ML. This repartition in 6 groups allow an easier description of the variability of the data set, but also helps to disentangle synopticity (there was a seasonal evolution during PERLE2 cruise) from mesoscale activity. For instance, group B gathers ST50, 104 and 108 which share highest dynamic heights (median -0.320 dyn m), and deepest depths of the isopycnal 29.05 (median 408 m) of the whole winter cruise (Table S1, Fig. 4b, c). Group B thus represents the most typical anticyclonic situations, with ST50 located at the center of the Ierapetra anticyclone, and ST104 and 108 along the anticyclonic side of the geostrophic jets entering in the Cretan Sea (Fig. 2, Fig. S3d). The ML in this group B was therefore characterized by the highest salinity (median 39.29) and temperature (median 16.9°C, Table S1, Fig. 4d) measured during PERLE2 cruise. Five stations constituted group C (ST21, 26, 35, 44, 75), showing intermediate depths of isopycnal 29.05 (median 212 m) and dynamic heights (median -0.39 dyn m). Stations from groups C to E were characterized by a progressive shallowing of the ML and of the isopycnal 29.05, and an increase of median temperature inside the ML (Fig. 4). Last, ST1, 13 and 15, which constituted group F, are located in the Cretan Sea or in the Kythira strait between the Aegean and

the Ionian Seas. They were sampled at the beginning of the cruise and all show deeper MLD, and lower median salinities and temperatures inside the ML (median 39.19 and 15.7°C, respectively, Table S1, Fig. 4, Fig. S4g, h, i).

425

3.3. Distribution of biogeochemical properties within the mixed layers

Depths of nutriclines varied among the different cruises and groups (Table S1, Fig. 4e, f). The deepest Ncline and Pcline were observed in stations situated within anticyclonic areas during the winter cruise (group B, with medians 211 and 257 m, respectively), followed by the well-mixed
430 stations at the beginning of the cruise (group F). The shallowest Pcline and Ncline were reached in groups D and E, although the Dunn test showed no significant differences among the 3 groups C, D, and E.

DIP varied in the nanomolar range, from 5 to 26 nM (Fig. 5c). Only stations of the group F, which were sampled at the beginning of the cruise in the Cretan Sea, had significantly (Kruskal-Wallis &
435 Dunn tests) higher DIP concentrations than the other groups (group F median of 23.3 nM compared to 8.4 to 10.2 nM for the others, Table S1, Fig. 5c). While DIP concentration was not particularly low in the autumn cruise (group A, Fig 5c), conditions were clearly N-depleted, with frequent subsurface NOx concentrations below the detection threshold of 0.01 µM (median in group A: 0.011 µM, Table S1, Fig. 5b). NOx concentrations were within the same order of magnitude in
440 stations belonging to groups B, C and D (Dunn test, Fig. 5b). Notably, NOx decreased at stations of group E (median 0.29 µM) (Table S1, Fig 5b). Keeping only data where NOx was above detection limits, NOx:DIP molar ratio was lower in autumn (median 1.5) compared to winter (range 32-79 according groups, Table S1).

DOP and L_{DOP} showed the lowest values in autumn (group A: medians 22 and 6 nM, respectively,
445 Dunn test, Fig. 5g, d) and the highest values in the well-mixed stations of the winter cruise (group F: medians 70 and 29 nM, respectively, Dunn test). The fraction of L_{DOP} in DOP exhibited large variability within each group, with values not significantly different in groups A, B and C (medians 23, 20 and 18%) and slightly higher in groups D, E and F (medians 33; 30 and 41%, respectively, Table S1). The different groups in winter show close DON medians (range 4.3-4.5 µM) that are
450 lower than during the autumn cruise (group A: 5.2 µM), which also showed the highest variability (Table S1, Fig. 5f). This was also the case for DOC, with a marked contrast between winter and autumn (median DOC: 57-65 M *versus* 80 µM, respectively), and a lower variability of DOC data in autumn (group A, Fig. 5e).

455 3.4. Distribution of populations and pigments within the mixed layers

Median abundances of *Prochlorococcus* observed within the ML were the lowest in autumn (Group A, PERLE1), at the time when those of *Synechococcus*-like and nano- and pico-eukaryotes were the highest (Fig. 6b, c, d, Table S2). In winter, abundances of all phototrophic populations tended to be higher in groups D and E (in stations sampled later in the cruise and in cyclonic conditions) compared to groups B and C (anticyclonic conditions). The median abundances of heterotrophic prokaryotes ranged from 3.3 to 4.2 x 10^5 cells mL^{-1} for all groups except for group D, which showed a peak of 6.7 x 10^5 cells mL^{-1} (Fig. 6e, Table S2).

Total chlorophyll a (Tchla) showed the highest median concentrations in groups D and E corresponding to winter, cyclonic conditions and shallow MLD. The lowest Tchla were observed in autumn within the Ierapetra gyre (group A, Fig 6). Pigment's distribution was used to tackle a finer distribution of phytoplankton populations. For instance, during strong mixed conditions in the north of Crete (group F), fucoxanthin and peridinin showed the highest relative indexes (ratios to Tchla), and so did the degradation index (Fig. S7a, b). In winter, 19'BF:Tchla ratio decreased from anticyclonic situations (groups B and C) to cyclonic ones (groups D and E) (Fig. S7f). While groups B and C in one hand, and D and E in the other hand, had similar standing stocks of Tchla (Fig. 6a), phytoplankton population showed taxonomic changes within these pairs. For instance, from group B to C, the peri:Tchla ratio increased while chlb:Tchla and 19'BF:Tchla decreased, suggesting a shift from micro to nanophytoplankton. From groups D to E dv-chla:Tchla, chlb:Tchla ratios and degradation index decreased while allo:Tchla ratio increased in good agreement with the observed decrease in the *Prochlorococcus* abundance and the increase in *Synechococcus* and Nanoeuk (Fig. 6, S7)

3.5. Distribution of phosphatase and BP activities inside the mixed layers

Within the ML, Km medians ranged from 1.3 to 6.6 µM for PDE and 0.063 to 0.22 µM for PME among the different groups (Table S2, Fig. 7c, d). Km PME were the lowest in autumn (Dunn test, group A median 0.063 µM) and reached their maximum in groups D and E (medians 0.20 and 0.22 µM, respectively). Km PDE were the lowest in winter in the well-mixed stations (Dunn test, group F, median 1.3 µM) but as Km PME, reached their maximum in groups D and E (6.3 and 6.6 µM, respectively).

Vm PME and Vm PDE showed the same trends among groups (Table S2, Fig. 7a, b): their medians were both minimal during well mixed, winter conditions (group F, Dunn test, Fig 7), coinciding with the highest DIP concentration (median 23 nM). Stations sampled in autumn (group A) showed the second lowest medians. The median values of Vm PDE and Vm PME were maximal in group E, although with the greatest variability. The ratio Vm PME:Vm PDE was slightly lower and less

variable in groups B, C, D and E (medians 0.46 to 0.64) compared to groups A and F (medians 0.97-1.14, Fig. 7g).

The partitioning of medians of biomass specific Vm PDE and PME within the ML in the different groups differed slightly from that of their volumetric Vm counterparts (Fig. 7 a, b *versus* Fig. 7 e, f). The highest median of biomass specific Vm was still obtained in group E and the lowest in group F for both enzymes (Table S2). However, the biomass specific Vm PME and Vm PDE, values were not different anymore between groups B, C and D (Dunn test), and these 3 groups exhibited the lowest median values, varying between 0.12 and 0.17 nmol P hydrolyzed $[\mu g\ C]^{-1}\ h^{-1}$ for PME and between 0.23 and 0.25 nmol P hydrolyzed $[\mu g\ C]^{-1}\ h^{-1}$ for PDE. The stations sampled in autumn (group A) became the second group showing high biomass specific activity after group E. The highest medians of heterotrophic prokaryotic production (BP), both bulk and cell-specific, were obtained in group D and E (Fig. 6g, h, Table S2).

3.6 Relationships between hydrological properties of the stations and biotic variables.

We computed direct correlations between hydrologic and biotic variables, considered as medians in the mixed layer (nutrient stocks, dissolved organic matter, abundances of microorganisms (Table S4) and algal pigments (Table S5). We also examined correlations with integrated abundances and stocks (Table S6). The correlation coefficients showed systematically opposite signs when gradient across isopycnals was used as a hydrological variable compared to the depth of nutricline. In most cases, median values of biotic parameters in the ML were more significantly, and more highly correlated with gradients across isopycnals than with the nutricline depth. This observation holds true whatever the method used to estimate ZNcline (based on the intercept of 0 NOx, or on the intercept of mean NOx in the ML, see paragraph. 3.1). Biotic variables were more frequently and more significantly correlated with H500 than with PISO or MLD.

4. Discussion

4.1 Mesoscale structures

In the EMS, the cyclonic Rhodes gyre and the anticyclonic Ierapetra gyre are some of the most frequently observed and best described structures (Salihoglu et al., 1990; Popov, 2004; Zodiatis et al., 2023), although there are also many other smaller eddies with varying size and life times (Barboni et al., 2023 and ref therein). In the area south of Crete, the Cretan cyclone and the Ierapetra anticyclone, for instance, are quasi-permanent features but may not form at particular years (Ioannou et al., 2017). The formation of the Ierapetra anticyclone occurs in the beginning of summer, and its maximum intensity is generally observed in October/November (Ioannou et al., 2017). While the life time of Ierapetra anticyclone is about one year, it may be seen for up to 3

years (Ioannou et al., 2017), while at some periods it may be no longer visible, or may be connected to the larger scale circulation variability of the eastern Mediterranean (Velaoras et al., 2019). As the energy supply becomes weaker, the anticyclone shifts to the south or southwest before collapsing (Popov, 2004). During our PERLE1 cruise in autumn, many stations were sampled in and around the Ierapetra anticyclone, which was particularly well marked and was probably at the peak of its intensity (Fig. 1). Five months later, it moved to the west, showing a reduction in size and intensity as seen during the PERLE2 cruise (Fig. 2) and only one station (ST50) is located inside it. In parallel with the weakening of the Ierapetra anticyclone, the cyclonic Rhodes gyre is expanding westwards to include a small anticyclone (AE, Fig. 2).

If the hydrological discontinuities were some factors explaining the repartition of the different groups in the PCA, in addition, medians of biogeochemical properties within the ML allowed separating some other groups. Stations were distributed as follows: i) according to the season (group A: autumn cruise vs other groups: winter cruise, discussed section 4.4.1) and ii) within the winter season, according to areas exhibiting clear cyclonic (groups D, E) or anticyclonic (group B) but also according temporal scales, as stations typical of a well-mixed water column in the Cretan Sea at the start of the cruise (group F, case discussed in section 4.3) or changes of biogeochemical properties after a short wind event (comparison of groups D and E, case developed section 4.4.2).

4.2 Integrated stocks and phytoplankton bloom across the different mesoscale structures

In this study, higher integrated nutrient stocks were measured at stations sampled at the extension of the Rhodes gyre (cyclonic, group E, 12-24 mmol DIP m^{-2}) than at ST50, ST104 and ST108 in anticyclonic areas (group B, 1.7-2.7 mmol DIP m^{-2}), in accordance with the shoaling of the nutriclines depths. This observation is in good agreement with the higher nutrient concentrations, higher biological activities and different phytoplankton communities already reported inside cyclonic gyres compared to anticyclonic eddies (Sweeney et al., 2003; Mouriño-Carballido and Mc Gillicudy, 2006; Belkin et al., 2022). In our study, integrated Tchla stocks reached > 60 mg m^{-2} at ST15 (group F, mixed conditions in Cretan Sea), ST50 as well as ST108 (group B, anticyclonic situation), ST80 (group E, cyclonic situation) although they were characterized by contrasted mesoscale structures. Indeed, high integrated Tchla stocks (70 mg m^{-2}) have already been observed in winter in an anticyclonic gyre, the Cyprus eddy in February 1989 when Tchla was distributed down to unusual deep layers (250 m, Krom et al 1992). Belkin et al. (2022) compared an anticyclonic (2 months old) and a cyclonic (13-month-old) eddy in the East Levantine Sea, during a period (late summer 2018) just before PERLE1 cruise (autumn 2018). Based on the comparisons of depth-integrated biogeochemical parameters down to 180 m, these authors showed higher nutrient concentrations, as well as an enhancement of dinoflagellates and prymnesiophytes growth, and

concomitant higher primary production, as well as higher production and growth rates of heterotrophic prokaryotes in the cyclonic eddy compared to the anticyclonic one. This dichotomy was not so marked in our study. Integrated BP (0-200 m) was elevated at ST80 and ST90 reaching 55 mg C m^{-2} d^{-1}, while at the other stations of the group E (ST94 and ST68) the integrated BP rates (26 and 30 C mg C m^{-2} d^{-1}, respectively) were close to the values obtained at the stations of the group B (31-40 mg C m^{-2} d^{-1}). Note, however, that we could not sample inside the core of the Rhodes gyre, and hence we may have missed the higher activities or higher integrated Tchla stocks, characteristic of the center of this gyre. Nevertheless, Tchla values within the ML reached 0.87 µg L^{-1} at ST80, which was higher than the maximum of 0.6 µg L^{-1} value recorded by the BGC Argo floats within the region under the Rhodes gyre influence (defined by D'Ortenzio et al. (2021) as the region where the annual satellite SST minima is less than 15°C). Primary production was indeed the highest at ST90 (group E, 509 mg C m^{-2} d^{-1}) under the influence of the Rhodes gyre.

At all the stations where both BP and PP were determined in winter (restricted to groups F, C and E) and assuming a bacterial growth efficiency of 10% for Hprok, the system was net autotrophic. A very low summer PP is consistently reported in the EMS (Reich et al., 2022: 48-113 mg C m^{-2} d^{-1} during stratified months), particularly in an anticyclonic area (Belkin et al., 2022: 36 mg C m^{-2} d^{-1}; Ierapetra gyre in autumn 2019, this study: 39-123 mg C m^{-2} d^{-1}). Belkin et al. (2022) measured PP of 191 mg C m^{-2} d^{-1} in a cyclone offshore the Israeli coast in summer, compared to 81 mg C m^{-2} d^{-1} in the adjacent waters, concurrently with PERLE 1 cruise (October 2018). In contrast, there is a paucity of *in situ* measurements in winter in the EMS, particularly in a cyclonic area like the Rhodes gyre. We estimated daily values of 131 mg C m^{-2} d^{-1} from PP hourly rates cited in Varkitzi et al. (2020), in March/April 2008, during an exceptional phytoplankton bloom in the South Aegean Sea. During a particularly intense vertical convective overturning in early 2012, Pedrosa-Pàmies et al. (2016) predicted 2.7 µM NO_3^- and 0.13 µM DIP within the Rhodes gyre using a biogeochemical model, and 1.9 µg chla L^{-1} through remote sensing of surface chlorophyll a. Vidussi et al. (2001) measured 4 µM NO_3^- and 32.9 mg chla m^{-2} from which, using a spectral photosynthesis model, they predicted PP rates as high as 420 mg C m^{-2} d^{-1}. Peaks of PP have scarcely been measured *in situ*, in the Rhodes gyre, like in Napolitano et al. (2000): 600 mg C m^{-2} d^{-1} in early March 1995 or 479 mg C m^{-2} d^{-1} in May 1996). One cannot preclude possible overestimations of PP values with the ^{14}C technique employing incubations in deck incubators, as phytoplankton cells in flasks are not submitted to the strong vertical mixing affecting cells under *in situ* conditions, as when ML reached deeper depths than the euphotic zone, particularly at the beginning of the cruise. Note that chlorophyll biomass was also reaching values around 0.2 to 0.4 µg Tchla L^{-1}, and hence we obtained chlorophyll-normalized production ranging between 19 and 30 µg C [µg Tchla]$^{-1}$ d^{-1},

595 which are not abnormal values for the Med Sea. For instance, Marañón et al. (2021) obtained a range of 20-40 µg C [µg Tchla]$^{-1}$ d^{-}1 in spring in the western MS at near-surface irradiance levels. In addition, as developed by Habib et al. (2023), the winter mixing 2018-2019 was particularly intense in terms of mixing compared to the other years between 2015 and 2021, and led to a strong bloom the following spring. In addition, D'Ortenzio et al. (2021) showed, using a Biogeochemical
600 Argo data set, that phytoplankton had already started to grow also outside of the Rhodes gyre since the beginning of February.

These observations, together with the high values of PP (360 – 509 mg C m^{-2} d^{-1}) that we measured evidenced a significant winter bloom, not only in the Rhodes gyre area but also all around Crete as well. Based on the above, more *in situ* measurements are needed in winter to assess the frequency
605 of such blooms in areas assumed to be 'non-blooming' according a satellite-based approach (D'Ortenzio and Ribera d'Alcalà, 2009). Below, we will develop on the particular case of the northwestern area of Crete (stations of the group F).

4.3 The mixing events as starters of successive winter blooms, the case of group F

610 During the PERLE 2 cruise (from February 27 to March 15), the Rhodes gyre area was affected by 3 major mixing events, leading to abrupt changes in the MLD. The deepest ML, around 200 m, was observed in the core of the Rhodes gyre at the end of February (Taillandier et al., 2022). Likewise, the 145 m median MLD, the rather homogeneous chlorophyll profiles and NOx concentrations reaching 1.1 µM that we observed at stations in the Cretan Sea (group F) also point to a very recent
615 mixing event in this area. Unfortunately, satellite images in the west Cretan Sea are too patchy and cloudy during that period to infer a bloom development (D'Ortenzio et al., 2021). However, E1-M3A mooring line near ST1 provided useful information on the 2019 seasonal trends of density and chlorophyll in the Cretan Sea around the sampling date of the stations of the group F (Fig. S8). The evolution of the potential density anomaly at different depths indicates important mixing of the
620 upper water column during winter 2019 in the Cretan Sea. In particular, mixing affected the water column down to 250 m at the PERLE2 cruise period (Fig. S8a). Chlorophyll fluorescence at 50 m has been increasing since mid-January 2019, reaching maximum values around mid-March, and remained more or less constant until mid-May before decreasing (Fig S8b). Short-term variations in chl fluorescence appear also most likely related to vertical movements of the DCM depth due to the
625 horizontal displacement of different mesoscale structures and/or occurrence of wind events at the buoy position. Before the sampling date of ST1 (February 27), two peaks of chlorophyll fluorescence are visible on February 12 and February 24. Chl fluorescence began to decrease 3 days before the sampling date of ST1. The high integrated Tchla stocks seen at the station of the group F (51-66 mg m^{-2}) are thus the trace of recent phytoplankton growth.

Pigments available at ST15 (sampled on 1st March) show high Fuco:Tchla and 19'BF:Tchla ratios compared to the other groups, suggesting the presence of pelagophytes. The chlb:Tchla, ratio was also high, with noticeable abundances of picoeukaryotes, which suggests a relative dominance of prasinophytes. Further, the high pigment degradation index (0.03, again the highest obtained during this cruise) suggests that phytoplankton cells were not particularly healthy, probably due to a recent strong mixing below the euphotic zone. The Cretan Sea buoy records and our data from the ST1, 13, and 15 (nutrients, chlorophyll stocks, and pigment's diversity) suggests that such intermittent periods of mixing occurring early in winter could also have triggered growth in the north-west of Crete before our sampling and the mixing event of the end of February. This has been observed before in February 2008 when, after a particularly intense winter convection, a phytoplankton bloom was detected in this region (Varkitzi et al., 2020), otherwise classified as a 'non-blooming area' (D'Ortenzio and Ribera d'Alcalà, 2009). These findings suggest that a significant, early winter bloom occurred in 2019 in the north western Crete area, emphasizing the need for further winter in situ measurements around Crete to refine bloom localization and frequency assessments in the eastern Mediterranean.

4.4 Biogeochemical dynamics in the mixed layer: autumn versus winter cruises

As developed above, integrated stocks or fluxes (down to 150 - 250 m) reflect mainly the downwelling or upwelling effects on Pcline and Ncline among the different structures, but cannot inform on the processes of acclimation and phylogenic successions of both phytoplankton and heterotrophic bacterioplankton within the mixed layer, which is depleted in nutrients most of the year in the EMS. For instance, in the study of Belkin et al. (2022), NOx and DIP concentrations were close to, or below, the detection limit of conventional analytical methods at all stations in the upper 100 m, whereas integrated values down to 180 m were highly contrasted between cyclonic and anticyclonic areas, as was also observed in our study by comparing integrated DIP or NOx stocks. Thus, in the need to better reveal community adaptations within the ML, we analyzed hereafter the variability of biogeochemical properties within the ML. We cross-compared here winter and autumn cruises, as well as the different hydrological structures, with a particular focus on the P cycle.

4.4.1 Comparison autumn-winter cruise: nutrients

In the EMS, there is, even in offshore sites not influenced by any mesoscale structure, a seasonal biogeochemical change between the mixed winter period (January - April) and the thermally stratified (May - December) period (Ben Ezra et al., 2021). Such seasonality is clearly visible in our study between group A (autumn cruise) and the other groups (winter cruise) in the PCA (Fig. 3).

The autumn situation was characterized by the vertical structure of the stations: shallower MLD, greater dynamic heights, deepest nitracline and the formation of a DCM around 100 m (Fig. S3), coupled to a bimodal picophytoplankton distribution, with *Synechococcus* in the ML and *Prochlorococcus* at the DCM depth (Van Wambeke et al., 2023).

Regarding nutrient concentrations, DIP exhibited median values around 8-10 nM, even during the autumn cruise (median 10 nM), with the notable exception of group F. The significantly higher median DIP concentration present in the ML at the beginning of the cruise in the stations of this group (20 nM) was probably due to the mixing event explained before. For instance, after the intense winter convection occurring in February 2008 (Varkitzi et al., 2020, DIP ranged ~ 60 nM in sea-surface of the Cretan Sea and in the western passage. Our DIP values are typical of phosphate-depleted waters in the EMS (Livanou et al., 2019; Oikonomou et al., 2020; Pulido-Villena et al. 2021; Ben Ezra et al., 2021). In comparison to the rather stable concentrations of DIP, NOx concentrations were mostly undetectable inside the ML in autumn whereas they were highly variable concentrations in winter, with maximum medians (1.10 µM) in group F, and minimum medians (0.29 µM) in group E (including ST80 in which NO_3^- decreased down to 0.03 µM). Consequently, in autumn the median ratio of NOx:DIP median (1.5) was lower than the Redfield 16:1 ratio, and higher in winter (32-79). Similar seasonality was also described in Reich et al. (2022) and Ben Ezra et al. (2021). Consequently, the phytoplankton in the ML during Feb-March and the October cruise differed in terms of nutrient limitation, being probably P-limited in winter and N-limited or N+P co-limited in autumn as already suggested (Zohary et al., 2005; Tanaka et al., 2011; Ben Ezra et al., 2021). However, heterotrophic bacteria and phytoplankton might not be limited on the same manner during the stratification period (Zohary et al., 2005), giving complexity to the limitation status in summer referring only on nutrient stocks. The only case of non-P limitation seems to have been reached in the group F: there, medians of DOP stocks and L_{DOP} were the highest in the ML, and phosphatase activities were the lowest, suggesting that the microorganisms in place could satisfy their P requirements from DIP utilization, and/or phytoplankton were stressed due to their large vertical displacements during the mixing event, so that the sources of DIP were higher than their sinks, explaining why there was still a 20 nM, detectable DIP concentration there.

4.4.2 Comparison of autumn and winter cruise: external fluxes, P stress, and microorganism's responses through phosphohydrolase activities

Even though very low and constant, the observation of DIP stocks in winter and autumn alone is not sufficient to predict the degree of P-limitation of the microorganisms (Tanaka et al., 2006). As

concentrations vary according to sources and sinks, low standing stocks could as well result from very high turnover rates and equally high consumption. We therefore examined a possible DIP supply to the ML through external fluxes (F). Keeping only the significant values of $\partial DIP/\partial \sigma$ calculated inside the P-depleted layer across the ML (Table S3), the averages were 296 ± 146 µmol DIP kg^{-1} in winter (n = 4) and 3.8 ± 0.02 µmol DIP kg^{-1} in autumn (n = 5). The higher $\partial DIP/\partial \sigma$ observed in winter suggests that higher vertical diffusion is higher in winter and also very variable between the different hydrological structures. However we are missing turbulent kinetic energy dissipation rate measurements, during both cruises to confirm this statement. We also suspect lateral advection to play an important role in DIP supply, as already demonstrated for DOC (Habib et al., 2023). Other external sources of DIP are atmospheric inputs, unfortunately not available for this cruise. Monthly averages and models of dry and wet deposition at Finokalia station, in Crete, suggest that atmospheric supply of DIP is lower in autumn than in the winter/spring season (Kanakidou et al., 2020), and so the difference in external supply of DIP between both cruises may be even higher.

Internal sources of DIP within the mixed layer are provided by the hydrolysis of DOP, via the synthesis of phosphohydrolases by microorganisms as a response to P stress. DOP, and in particular L_{DOP}, in the ML were less concentrated during the autumn cruise, pointing to an efficient utilization of organic P by microorganisms.

Maximum Vm rates were obtained at the stations under the Rhodes gyre influence (group E) during the winter cruise. Compared to the autumn situation where a low amount of living biomass is present, relative rates in group E (biomass specific Vm PME and PDE) remained about twice as high as the values obtained in autumn. This difference could be even higher considering that temperature was about 10°C higher in autumn, so that based on an assumed Q10 (the number of times that a 10°C change in temperature results in changing the Vm rate) around 2 (Apple et al., 2006), specific Vm rates would be only 1/4 of the values obtained in group E based on equal temperatures. Several explanations can be put forward for this difference. First, in line with Thingstad et al. (2005), the present results point to a co-limitation of microbial populations by N+P, and not P alone, in autumn. We postulate that this co-limitation might have affected phosphatase synthesis, as the availability of N is also necessary for cells to produce these enzymes. In addition, microorganisms have evolved different strategies to cope with P scarcity. In winter, expression of phosphatases, but also phagotrophic predation were probably the strategies used by the pico and nano phytoeukaryotes. Indeed those abundant populations were probably dominated by dinoflagellates and green algae, as seen from peri/Tchla and chlb/Tchla ratios which peaked within the Rhodes gyre (groups D and E). Those populations are mixotrophic protists capable to ingest

Hprok under P limitation (Duhamel et al., 2019). In autumn, prokaryotic phytoplankton (*Synechococcus, Prochlorococcus*) are adapted to nutrient-limiting conditions due to their higher surface:volume ratio. Also, nutrient limitation is perceived as a stress that triggers a number of genetic regulations of which the most widespread is an increase in the synthesis of high affinity phosphate-specific transporters (Rosenberg et al., 1977; Suzuki et al., 2004; Lomas et al., 2014). Another response to P stress involves the decrease in cell P quota through the substitution of phospholipids with sulfolipids, which seems to be only observed in the phytoplankton but not in the heterotrophic prokaryotes (Van Mooy et al., 2009). Moreover, the median Km PME was lower during the autumn cruise (group A) suggesting that the more acute P-limiting conditions in autumn selected for organisms with a higher affinity for P-monoesters. This observation is in good agreement with the lower medians of L_{DOP} concentrations in PERLE1 (6 nM) compared to PERLE2 (medians 11 to 29 nM according the different groups) and thus varied within the ML more dynamically than DIP. Similarly to what has been reported in both the Sargasso Sea, where surface DIP values can be very low all year round (Lomas et al., 2010), and a coastal zone in eastern Mediterranean (Ben Ezra et al., 2021), DOP concentrations displayed a seasonal pattern with higher concentrations in winter than in summer months. Our results further indicate that such pattern also applies to L_{DOP}.

Thus, microbial responses to phosphorus stress thus differed between seasons, with an autumn situation characterized by a N+P co-limitation status, dominance of picoplanktonic populations showing efficient utilization of DIP through probable reduction of P requirements and high affinity of DIP uptake systems. The winter situation is characterized by a P limitation status. During the peak of the bloom, two non-mutually exclusive scenarios were proposed: i) dominance of mixotrophic, phytoplankton probably able to exert phagotrophic predation. ii) the populations present expressed more phosphohydrolase activities.

4.5 Biogeochemical dynamics in the mixed layer in winter: the Rhodes gyre

4.5.1. Primary production and phytoplankton community structure

Stations belonging to groups D and E all are all in cyclonic areas: Pcline and Ncline there are much shallower than in stations of groups B and C. In groups D and E, phytoplankton biomass also reached maximum values in the ML, as seen both in the chlorophyll stocks (Tchla around 0.42 µg L^{-1}) and specific abundances of Picoeuk, Syn and Proc. The enhanced primary production and phytoplankton biomass observed in cyclonic areas due to the 'doming' structure has been well described previously (Mouriño-Carballido and McGillicuddy, 2006; Belkin et al., 2022), and has been reported in the Rhodes gyre for a long time. Note that among all the hydrological variables tested, the dynamic topography (H500) appears as the most suitable parameter to reveal the

relationship between cyclonic and anticyclonic structure and populations abundances or diagnostic pigments, in comparison to the MLD or the depth of isopycnal 29.05 kg m^{-3} (PISO). On the other hand, phytoplankton groups or pigments were also better correlated to the gradients across isopycnals than to the depths of nutriclines.

Maximum primary production was reached at station 90 (509 mg C m^{-2} d^{-1}; 11-16 µgC L^{-1} d^{-1} in the ML). Maximum Tchla stocks were reached at station 80 (65 mg Tchla m^{-2} and 0.9 µg Tchal L^{-1} in the ML, at a time when NOx were already mostly consumed (0.03 µM at ST80) while a few days before they reached 3.5 µM as seen from Biogeochemical Argo data set (Biogeochemical Argo are equipped with a nitrate sensor SUNA, D'Ortenzio et al., 2021).

∂DIP/$\partial\sigma$ gradients at the Pcline depth were higher (medians in groups D and E: 2753 and 2410 µmol kg^{-1}, respectively) than in the adjacent stations out of the Rhodes gyre influence (group C). The same applies when comparing the ∂DIP/$\partial\sigma$ gradient in the P depleted layer between ST21 (group C) and ST116 (group D, Table S3). The phytoplankton bloom in the Rhodes gyre might thus have been favored by a simultaneous higher vertical supply of DIP from the phosphacline and a shallower ML. Accordingly, abundances of picoeukaryotes and *Prochlorococcus* increased in both groups (Fig. 6). Peridinin and fucoxanthin increased too, both in absolute values and relatively to Tchla, whereas 19'HF was constant, or decreased compared to groups B and C, suggesting dinoflagellates' and diatoms' growth in groups D and E. This microphytoplankton growth may be indirectly supported by PP size fractionation results (data not shown). At ST90 (group E) where the highest PP values were recorded (509 mg C m^{-2} day^{-1}) picoplankton relative contribution to total PP (< 2 µm fraction) was the lowest in the surface layers (33% as compared to 47%-64% in the other stations) whereas the opposite was seen for high-sized nanoplankton and microplankton (> 5 µm fraction: median 25% compared to 16-24% in the other stations). Finally, heterotrophic prokaryotes also benefited from phytoplankton by-products through excretion or grazing, as BP cell specific activities were also higher in groups D and E than in groups B and C. More intense heterotrophic pathways, through BP and nanozooplankton grazing, might also enhance DIP regeneration inside the ML to fill phytoplankton P requirements.

4.5.2 Effect of a short time-scale mixing event within the Rhodes gyre.

Some differences observed between groups D and E were attributed to a temporal evolution, as ST80 (group E) and ST111 (group D) were sampled at the same location, 4 days apart (ST80: 10 March, ST111: 14 March). Likewise, ST90 (group E) and ST116 (group D) are at the same location but sampled with 3 days apart (ST90: 12 March, ST116: 15 March. On the 13th of March a low intensity, brief mixing event occurred, as the meteorological sensors onboard the ship indicated a strong drawdown of air pressure from 1020 to 1000 mbars, and wind speed up to 30 knots after a

relative calm period (Taillandier et al., 2022). In both couples of stations, ML deepened, and sea surface temperature decreased about 0.4 °C, resulting in an injection of NOx (from 0.03 to 0.8 µM between samplings at ST80 and ST111, and from 0.23 to 0.6 µM between samplings at ST90 and ST116). At ST111 and 116 (reflected by group D) the bulk, but also the biomass specific Vm PME and PDE rates decreased and reached the same order of magnitude than in the stations of group C (Table S2), also suggesting a recent supply of DIP. In particular, the Pcline depth was only at 37 m at ST80 and thus the mixing event reached the Pcline, suggesting injection of DIP as well, but after 5 days (ST111) DIP concentration was still around 12 nM in the ML. This suggests that P limitation status inside the ML was very dynamic and could not be revealed by the changes in DIP stocks. The consequence of this P regime shift was analyzed in terms of phytoplankton and hprok distributions. The mixing process 'diluted' some phytoplankton groups that had started to stratify before the mixing event, as seen from the decreases in *Synechococcus* and nanoeukaryotes' abundances in the ML. Concomitantly, the short term mixing also uplifted deeper *Prochlorococcus* towards the ML. It is unlikely that Proc grew after NOx enrichment as this organism essentially uses ammonium, and usually occupies different niches than Syn during the stratification period in the EMS (Syn at the surface, Proc at depth in all types of mesoscale structures; Mella-Flores et al., 2011; Belkin et al., 2022). This typical vertical segregation was also seen in the present study in the Ierapetra gyre in autumn (Van Wambeke et al., 2023). As seen in Reich et al. (2021) and in the E group, this stratification of cyanobacterial populations began early in the winter. This mixing trend of phytoplankton at stations that were beginning to stratify within the euphotic zone was also reflected by some changes in pigments ratios in the ML (chlb:Tchla and 19'BF:Tchla increased, allo:Tchla decreased at ST111 and 116 in comparison to ST80 and 90). This was concomitant with an increase in the pigment degradation index indicating stressed phytoplankton (Fig. S5h). In contrast, the abundances of hprok were higher in the ML of ST111 and 116 (Fig. 6e). It has been shown that hprok outcompete phytoplankton after addition of low concentrations of DIP (< 35 nM, Rahav et al., 2021; 100 nM, Pitta et al. 2016). The interpretation of our *in situ* data, in addition to dilution effects, is further complicated by the rapid responses of microorganisms (a couple of days) and a delayed response of phytoplankton compared to that of heterotrophic prokaryotes, as seen for example *in situ* after dust deposition events (Rahav et al., 2016; Van Wambeke et al., 2021). Cell quotas can also change very rapidly as suggested by the 'tunneling theory' by Thingstad et al. (2005) that cannot be inferred simply based on abundances. This example showed the immediate (few days) effects of small mixing events that influenced phytoplankton and hprok competition and distribution within the ML, as well as their rapid response to P flux as seen from variation of phosphatases.

These observations highlight i) the high phytoplankton bloom occurring within the Rhode gyre in winter 2019, ii) the intricate interplay between short-term wind mixing events, nutrient availability, and microbial community responses within the ML, contributing to our understanding of seasonal variability in P cycle and phytoplankton communities within the Rhodes gyre during winter.

5. Conclusion

In this study, we report the changes in hydrological and biogeochemical properties observed during two cruises conducted in autumn and winter 2018-2019 in the Eastern Mediterranean Sea. The EMS is a typical, low-nutrient, low-chlorophyll area with a believed, low productivity consequent to nearly exhausted phosphate standing stocks within epipelagic waters. Our data set evidenced an important, winter phytoplankton bloom (Tchla reached up to 65 mg C m^{-2} and PP 509 mg C m^{-2} d^{-1}) not only in the vicinity of the Rhodes gyre, but also all around the Crete island area, that challenges the current understanding of biogeochemical processes in the EMS. We show that winter, mixing episodes have a significant role as they transiently bring the nitracline closer to the surface, relaxing nitrate limitation. Still, the phosphacline most often remains out of reach for microbial communities in the mixed layer, leaving the system in a severe, P-limited state. We used phosphomonoesterase and phosphodiesterase kinetics as tracers of P availability. Results point out distinct microbial responses to phosphorus stress between seasons. We show that the transient supply of N in winter leveraged P limitation by supporting high specific activities. The highest biomass-specific phosphohydrolase activities were recorded in the Rhodes Gyre during the phytoplankton bloom: the partial resupply of nitrate facilitated the dominance of nano and pico eukaryotes as green algae and dinoflagellates with probable bacterivory abilities. In contrast, the co-limitation by NO3 and DIP in autumn drove the system towards the dominance of smaller cells with a higher resource-use efficiency through a probable reduction of their P requirements. Some stations were sampled both before and after a mixing event in places influenced by the Rhodes gyre. During these 3-4 days intervals, populations present in the ML changed, as well as their physiology, as tracked by the pigment degradation index. Phosphatase rates decreased after the mixing event, showing immediate responses of microorganisms to the transient, increased P supply. The combination of different tools used to characterize the hydrological structure showed the relevance to consider H500 rather than MLD to infer relationships with phytoplankton population and diversity, and to use gradients across isopycnals rather than the nutricline depths. Overall, results highlight how the coupled influence of the hydrological structure and biological responses at mesoscale drives microorganisms' dynamics and the P cycle in the upper water column.

Acknowledgements

This study is a contribution of the PERLE project, a joint initiative of the 'Chantier Méditerranée' MERMEX supported by CNRS-INSU, IFREMER, CEA, and Météo-France as part of the program MISTRALS coordinated by INSU. PERLE1 (PROTEVS cruise) was also partly managed and founded by the 'Service Hydrographique et Océanographique de la Marine' – SHOM, Brest, France (funded by the French DGA). Pigments analysis of PERLE2 cruise were paid by the Equipex Naos program. We warmly thank many persons for their help on board and at the laboratory: Frank Dumas (chief scientist of PERLE1 cruise), Florian Voron and Sandra Nunige (for nanoP analysis and improvements), Sophie Guasco and Thibaut Wagener (for help in PDE PME measurements), David Pecqueur, Christophe Salmeron, Morgane Didry (for flow cytometry analyses), Olivier Crispi, Paul Labatut, Barbara Marie, Eric Maria (for nutrients and DOM sampling as well as ammonium analyses), Fabrizio D'Ortenzio (for pigment's sampling during PERLE2 cruise), Joelle Salaun (for pigment's sampling and analysis of PERLE1 cruise) and Patrick Raimbault (for 13C/15N teaching and analysis by mass spectrometry). We thank the services provided by 3 platforms (SAPIG https://lov.imev-mer.fr/web/facilities/sapigh/, BioPic https://www.obs-banyuls.fr/fr/rechercher/plateformes/biopic.html, PRECYM https://precym.mio.osupytheas.fr/) for chlorophyll and flow cytometry analyses. We acknowledge the support of POSEIDON Monitoring, Forecasting and Information System for the Greek Seas managed by HCMR (https://poseidon.hcmr.gr) who gave access to the E1-M3A mooring data. We thank two anonymous reviewers: their suggestions and comments strongly improved the final version of the paper.

Sample Credit author statement

France Van Wambeke: Conceptualization, Methodology, Investigation, Vizualisation, Writing – Original draft, **Pascal Conan**: Project administration, Funding acquisition, Conceptualization, Validation, **Mireille Pujo-Pay**: Investigation, Writing – Review and Editing, **Vincent Taillandier**: Investigation, Writing – Review and Editing, **Xavier Durrieu de Madron**: Project administration, Funding acquisition, Visualization, Writing – Review and Editing**, Stella Psarra**: Investigation, Writing - Review & Editing, **Sophie Rabouille** Investigation, Writing - Review & Editing, **Chloe Baumas**: Formal analysis, **Elvira Pullido-Villena:** Investigation, Writing – Review and Editing.

Data access

The two images of sea surface temperature are distributed by CMEMS under doi 10.48670/moi-00171. Data collected by the two oceanographic cruises are available at the operational oceanographic data center Coriolis (https://www.coriolis.eu.org/Data-Products/Data-Delivery/Mediterranean-Data-selection). The time series of M1-M3A mooring is accessible at https://apps.poseidon.hcmr.gr/webapp/poseidon_db/.

Competing interest's statement

The authors have no competing interests to declare

Figure captions.

Fig. 1 Mean Dynamic Topography (MDT, cm) and absolute geostrophic velocities during the PERLE 1 cruise period (11-20 october 2018) in the eastern Mediterranean. Sampled stations are indicated by dots and their numbers. Maximum speed is 60 cm s^{-1}. The main cyclonic features are designated as RG: Rhodes Gyre, CCG: Cretan Cyclonic Gyre, MC: Mirtoan West Cretan Cyclone, CC: Cretan Cyclone. The main anticyclonic features are designated as: IE: Ierapetra Eddy; MM: Mersa-Matruh, PA: Pelops Anticyclone. Data originate from CMEMS.

Fig. 2 Mean Dynamic Topography (MDT, cm) and absolute geostrophic velocities during the PERLE 2 cruise period (27 February – 15 March 2019) in the eastern Mediterranean. Sampled stations are indicated by dots and their numbers. Maximum speed is 45 cm s^{-1}. The main cyclonic features are designated as CCG: RG: Rhodes Gyre, Cretan Cyclonic Gyre, WCA: West Cretan Anticyclone, PA: Pelops Anticyclone; CC: Cretan Cyclone. The main anticyclonic features are designated as: IE: Ierapetra Eddy; MM: Mersa-Matruh; AE: Anticyclonic Eddy. Data originate from CMEMS.

Fig. 3 Principal component analysis plotted along the 2 first axes PC1 and PC2. Blue: 27 stations, (letters refers to the different groups; see Table 1 and text); red: the 22 variables used in the PCA (medians within the ML including abundances of *Synechococcus*-like cells (Syn), *Prochlorococcus*-like cells (Proc), eukaryotic picophytoplankton (Pico-euk), eukaryotic nanophytoplankton (nano-euk), heterotrophic prokaryotes (hprok), DIP, DOP, L_{DOP}, NOx, Vm and Km of PME and PDE, biomass specific Vm PDE (sp Vm PDE) and PME (sp Vm PME) as well as depth of the ML (MLD), depth of isopycnal 29.5 (PISO), dynamic height at 500 dbars (H500), depth of phosphacline (Z Pcline) and nitracline (Z Ncline), DIP and NOx gradients accross isopycnals (∂DIP/$\partial\sigma$) , ∂NOx/$\partial\sigma$); green: the 9 supplementary variables (medians within ML including Salinity (SAL) temperature (temp), density excess (sigma), all phytoplankton C biomass (phyto-C), abundances of HNA, LNA, Crypto-like cells) as well as DIP-depth and NOx depth gradients (grad DIP-Z, grad NOx-Z).

Fig 4. Box-plots distribution of some physical characteristics (mixed layer depth, dynamic height at 500dbar, depth of isopycnal 29.05, temperature within the ML layer, phosphacline and nitracline depths) among the different groups sorted according the ACP results: group A stations of the autumn cruise (PERLE 1, 11 stations), group B (stations 50, 104, 108), group C (stations 21 16 35

44 58 75), group D (stations 58 111 116) group E (stations 68 80 90 84), group F (1 13 15). Boxes show medians (horizontal black bar) and IQR (inter quartile ranges), whiskers show 1.5 x IQR of the lower and upper quartiles; outliers extend to the data range. Sombol 'o' denotes data included in the interval +- 3 x IQR and '*' values out of the interval +- 3 x IQR. Means are also indicated (red crosses). The series of symbols α, β γ... design groups that were not statistically different between themselves after the Dunn test ($p > 0.05$). Two stations have missing data (L_{DOP} for st 16 PERLE1, hprok abundance for st 58 PERLE2,) and were not included in the PCA, for statistics they were included in groups A and D a posteriori, in accordance to their non-missing biogeochemical characteristics.

Fig. 5. Box plots distribution of some biogeochemical characteristics within the mixed layer Silicates (Si), nitrate + nitrite (NOx), dissolved inorganic phosphate (DIP), Labile DOP (L_{DOP}), dissolved organic carbon (DOC) nitrogen (DOM) and phosphorus (DOP) among the different groups sorted according the PCA results: group A stations of the autumn cruise (PERLE 1, autumn cruise), group B to group F (winter cruise). Description of box plots, dots, cross, and letters as written in the legend of Fig. 4.

Fig. 6. Box plots distribution of some flow cytometric groups within the mixed layer (abundances of Prochorococcus, Synechococcus, autotrophic pico -and nano-eukaryotes, heterotrophic prokaryotes) as well as Total Chlorophyll a, heterotrophic prokaryotic production and cell specific prokaryotic production among the different groups sorted according the PCA results (see Table 1 and Fig 3). group A: stations of the autumn cruise, groups B to F (stations of the winter cruise). Description of box plots, dots, cross, and letters as written in the legend of Fig. 4.

Fig. 7. Box plots distribution of phosphomonoesterase (PME) and phosphodiesterase (PDE) kinetic parameters Vm and Km, as well as their biomass-specific Vm, and their ratio (Vm PDE:Vm PME) among the different groups sorted according the ACP results: group A stations of the autumn cruise (PERLE 1, autumn cruise), group B to group F (winter cruise). Description of box plots, dots, cross, and letters as written in the legend of Fig. 4.

References

Aminot, A., Kérouel, R., 2007. Dosage automatique des nutriments dans les eaux marines. in: Méthodes d'analyses en milieu marin, edited by: IFREMER, 188 pp.

Apple, J. K., del Giorgio, P. A., Kemp, W. M., 2006. Temperature regulation of bacterial production, respiration, and growth efficiency in a temperate salt-marsh estuary. Aquat. Microb. Ecol. 43, 243-254.

Barboni, A., Coadou-Chaventon, S., Stegner, A., Le Vu, B., Dumas, F., 2023. How subsurface and double-core anticyclones intensify the winter mixed-layer deepening in the Mediterranean Sea. Ocean Sci. 19: 229–250. https://doi.org/10.5194/os-19-229-2023

Belkin, N., Guy-Haim, T., Rubin-Blum, M., Lazar, A., Sisma-Ventura, G., Kiko, R., Morov, A.R., Ozer, T., Gertman, I., Herut, B., Rahav, E., 2022. Influence of cyclonic and anticyclonic eddies on plankton in the southeastern Mediterranean Sea during late summertime. Ocean Sci. 18, 693-715. https://doi.org/10.5194/os-18-693-2022

Bellacicco, M., Volpe, G., Colella, S., Pitarch, J., Santoleri, R., 2016. Influence of photoacclimation on the phytoplankton seasonal cycle in the Mediterranean Sea as seen by satellite. Remote Sens/ Environ. 184, 585-604. https://doi.org/10.1016/j.rse.2016.08.004

Ben-Ezra, T., Krom, M., D., Tsemel, A., Berman-Frank, I., Herut, B., Lehahn, Y., Rahav, E., Reich, T., Thingstad, T.F., Sherr, D., 2021. Seasonal nutrient dynamics in the P depleted Eastern Mediterranean Sea. Deep-Sea Res. Part I 176, article 103607, https://doi.org/10.1016/j.dsr.2021.103607, 2021.

Cauwet, G., 1999. Determination of dissolved organic carbon (DOC) and nitrogen (DON) by high temperature combustion. In: Methods of seawater analysis, 3rd Edn., edited by Grashoff, K., Kremling, K., Ehrhard, M., 407–420.

Céa, B., Lefèvre, D., Chirurgien, L., Raimbault, P., Garcia, N., Charrière, B., Grégori, G., Ghiglione, J.-F., Barani, A., Lafont, M., Van Wambeke, F., 2014. An annual survey of bacterial production, respiration and ectoenzyme activity in coastal NW Mediterranean waters: temperature and resource controls. Environ. Sci. Pollut. Res., https://doi.org/10.1007/s11356-014-3500-9

Crise, A., Allen J.I., Baretta, J., Crispi, G., Mosetti, R., Solidoro, C., 1999. The Mediterranean pelagic ecosystem response to physical forcing. Prog. Oceanogr. 44, 219-243. https://doi.org/10.1016/s0079-6611(99)00027-0

D'Ortenzio, F., Ribera d'Alcalà, M., 2009. On the trophic regimes of the Mediterranean Sea: a satellite analysis. Biogeosciences 6, 139–148. https://doi.org/10.5194/bg-6-139-2009

D'Ortenzio, F., Iudicone, D., de Boyer Montegut, C., Testor, P., Antoine, D., Marullo, S., Santoleri, R., Madec, G., 2005. Seasonal variability of the mixed layer depth in the Mediterranean Sea as derived from in situ profile, Geophys. Res. Lett. 32, 1–4. https://doi.org/10.1029/2005GL022463

D'Ortenzio, F., Taillandier, V., Claustre, H., Coppola, L., Conan, P., Dumas, F., Durrieu de Madron, X., Fourrier, M., Gogou, A., Karageorgis, A., Lefevre, D., Leymarie, E,. Oviedo, A.,, Pavlidou, A., Poteau, A., Poulain, P.M. Prieur, L., Psarra6, S., Puyo-Pay, M., Ribera d'Alcalà, M., Schmechtig, C. Terrats, L., Velaoras, D., Wagener, T., Wimart-Rousseau, C., 2021. BGC-Argo floats observe nitrate injection and spring phytoplankton increase in the surface layer of Levantine Sea (Eastern Mediterranean). Geophys. Res. Lett. 48, e2020GL091649. https://doi.org/10.1029/2020GL091649

Djaoudi, K., Van Wambeke, F., Barani, A., Hélias-Nunige, S., Sempéré, R., Pulido-Villena, E., 2018a. Atmospheric fluxes of soluble organic C, N, and P to the Mediterranean Sea: Potential biogeochemical implications in the surface layer. Prog. Oceanog., Mermex special issue 163, 59-69. https://doi.org/10.1016/j.pocean.2017.07.008

Djaoudi, K., Van Wambeke, F., Coppola, L., D'Ortenzio, F., Helias-Nunige, S., Raimbault, P., Taillandier, V., Testor, P., Wagener, T., Pulido-Villena, E., 2018b. Sensitive Determination of the Dissolved Phosphate Pool for an Improved Resolution of Its Vertical Variability in the Surface Layer: New Views in the P-Depleted Mediterranean Sea. Front. Mar. Sci. 5, 234. https://doi.org/10.3389/fmars.2018.00234

Duhamel, S., Kim, E., Sprung, B., Anderson, O.R., 2019. Small pigmented eukaryotes play a major role in carbon cycling in the P-depleted western subtropical North Atlantic, which may be supported by mixotrophy. Limnol. Oceanogr. 64, 2424–2440. https://doi.org/10.1002/lno.11193

Dunlap, P. V., Callahan, S. M., 1993. Characterization of a Periplasmic 3':5'-Cyclic Nucleotide Phosphodiesterase Gene, cpdP, from the Marine Symbiotic Bacterium *Vibrio fischeri*, J. Bact. 175, 4615-4624, https://doi.org/10.1128/jb.175.15.4615-4624.1993

Durrieu de Madron, X., Mermex Group, 2011. Marine ecosystems' responses to climatic and anthropogenic forcings in the Mediterranean, Prog. Oceanogr. 91, 97-166. https://doi.org/10.1016/j.pocean.2011.02.003

Ediger, D, Yilmaz, A., 1996. Characteristics of deep chlorophyll maximum in the Northeastern Mediterranean with respect to environmental conditions. J. Mar. Syst. 9, 291-303. https://doi.org/10.1016/S0924-7963(96)00044-9

Habib, J., Ulses C., Estournel, C., Fakhri, M., Marsaleix, P., Pujo-Pay, M., Fourrier, M., Coppola, L., Mignot, A., Mortier, L., Conan, P., 2023. Seasonal and interannual variability of the pelagic ecosystem and of the organic carbon budget in the Rhodes Gyre (eastern Mediterranean): influence of winter mixing. Biogeosciences 20, 3203-3228. https://doi.org/10.5194/bg-20-3203-2023.

Holmes, R.M., Aminot, A., Kérouel, R., Hooker, B., Peterson, B.J., 1999. A simple and precise method for measuring ammonium in marine and freshwater ecosystems. Can. J. Fish. Aquat. Sci. 56, 1801–1808. https://doi.org/10.1139/f99-128

Hoppe, H.-G., 1983. Significance of exoenzymatic activities in the ecology of brackish water: measurements by means of methylumbelliferyl-substrates, Mar. Ecol. Prog. Ser. 11, 299-308.

Huang, K., Zhuang, Y., Wang, Z., Ou, L., Cen, J., Lu, S., Qi, Y., 2021. Bioavailability of Organic Phosphorus Compounds to the Harmful Dinoflagellate Karenia mikimotoi, Microorganisms 9, 1961. https://doi.org/10.3390/microorganisms9091961

Ioannou, A., Stegner, A., Le Vu, B., Taupier-Letage, I., Speich, S., 2017. Dynamical evolution of intense Ierapetra eddies on a 22 year long period. J. Geophys. Res.: Oceans 122, 9276–9298. https://doi. org/10.1002/2017JC013158

Kanakidou, M., Myriokefalitakis, S., Tsagkaraki M., 2020. Atmospheric inputs of nutrients to the Mediterranean Sea. Deep Sea Res. Part II 171, 104606. https://doi.org/10.1016/j.dsr2.2019.06.014

Kirchman, D. L., 1993. Leucine incorporation as a measure of biomass production by heterotrophic bacteria. In: Handbook of methods in aquatic microbial ecology, edited by: Kemp, P.F., Sherr, B.F., Sherr, E.B. and Cole, J.J., Lewis, Boca Raton, 509-512.

Klein, B, Roether W, Kress, N, Manca B. B., Ribera d'Alcalà, M., Souvermezoglou, E., Theocharis, A., Civitarese, G., Luchetta, A., 2003. Accelerated oxygen consumption in eastern Mediterranean deep waters following the recent changes in thermohaline circulation. J. Geophys.Res.: Oceans 108**,** C9. https://doi.org/10.1029/2002JC001454

Krom, M., Brenner, S., Kress, N., Neori, A., Gordon, L.I., 1992. Nutrient dynamics and new production in a warm-core eddy from the Eastern Mediterranean Sea. Deep Sea Res. 39, 467-480. https://doi.org/10.1016/0198-0149(92)90083-6

Krom, M., Kress, N., Berman-Frank, I., Rahav, E., 2014. Past, Present and Future Patterns in the Nutrient Chemistry of the Eastern Mediterranean. The Mediterranean Sea: Its history and present challenges, edited by: S. Goffredo and Z. Dubinsky, Dordrecht, Springer Netherlands**:** 49-68. https://doi.org/10.1007/978-94-007-6704-1_4

Livanou, E., Lagaria, A., Santi, I., Mandalakis, M., Pavlidou, A., Lika, K., Psarra, S., 2019. Pigmented and heterotrophic nanoflagellates: Abundance and grazing on prokaryotic picoplankton in the ultra-oligotrophic Eastern Mediterranean Sea. Deep-Sea Res. Part II 164, 100-111.

Lomas, M. W., Burke, A. L., Lomas, D. A., Bell, D. W., Shen, C., Dyhrman, S. T., Ammerman, J. W., 2010. Sargasso Sea phosphorus biogeochemistry: an important role for dissolved organic phosphorus (DOP), Biogeosciences 7, 695–710. https://doi.org/10.5194/bg-7-695-2010.

Lomas, M. W., Bonachela, J. A., Levin, S. A., Martiny, A. C., 2014. Impact of ocean phytoplankton diversity on phosphate uptake. Proc. Natl. Acad. Sci. 111, 17540-17545. https://doi.org/10.1073/pnas.1420760111.

Luo, H., Benner, R., Long, R. A., Hu, J., 2009. Subcellular localization of marine bacterial alkaline phosphatases. Proc. Natl. Acad. Sci. 106, 21219-21223. https://doi.org/10.1073/pnas.0907586106, 2009.

Maixandeau, A., Lefèvre, D., Fernandez, C., Sempéré, R., Sohrin, R., Ras, J., Van Wambeke, F., Caniaux, G., Quéguiner, B., 2005. Mesoscale and seasonal variability of community production and respiration in the surface waters of the N.E. Atlantic Ocean. Deep-sea res. Part I 52, 663-1676. https://doi.org/10.1016/j.dsr.2005.03.007

Marañón, E., Van Wambeke, F., Uitz, J., Boss, E. S., Dimier, C., Dinasquet, J., Engel, A., Haëntjens, N., Pérez-Lorenzo, M., Taillandier, V., Zäncker, B., 2021. Deep maxima of phytoplankton biomass, primary production and bacterial production in the Mediterranean Sea, Biogeosciences 18, 1749–1767. https://doi.org/10.5194/bg-18-1749-2021

Marie, D., Partenski, F., Jaquet, S., Vaulot, D., 1997. Enumeration and cell cycle analysis of natural population of marine picoplankton by flow cytometry using the nucleic acid stain SYBR green I. Appl. Environ. Microbiol. 63, 186-193.

Marie, D., Simon, N., Guillou, L., Partensky, F., Vaulot, D., 2000. Flow Cytometry Analysis of Marine Picoplankton, in Living Color: Protocols in Flow Cytometry and Cell Sorting, edited by: Diamond R. A. and Demaggio S., Springer, Berlin, 421–454, eBook ISBN 978-3-642-57049-0

Mayot, N., D'Ortenzio, F., Ribera d'Alcalà, M., Lavigne, H., Claustre, H., 2016. Interannual variability of the Mediterranean trophic regimes from ocean color satellites. Biogeosciences 13, 1901-1917. https://doi.org/10.5194/bg-13-1901-2016

Mella-Flores, D., Mazard, S., Humily, F., Partensky, F., Mahé, F., Bariat, L., Courties, C., Marie, D., Ras, J., Mauriac, R., Jeanthon, C., Mahdi Bendif, E., Ostrowski, M., Scanlan, D. J., Garczarek, L., 2011. Is the distribution of *Prochlorococcus* and *Synechococcus* ecotypes in the Mediterranean Sea affected by global warming? Biogeosciences 8, 2785–2804. https://doi.org/10.5194/bg-8-2785-2011

Moran, X.A., Taupier-Lepage, I., Vasquez-Dominguez, E., Ruiz, S., Arin, L., Raimbault, P., Estrada, M., 2001. Physical-biological coupling in the Algerian Basin (SW Mediterranean): Influence of mesoscale instabilities on the biomass and production of phytoplankton and bacterioplankton. Deep-Sea Res. part I 48, 405-43.

Mouriño-Carballido, B., McGillicuddy Jr, D. J., 2006. Mesoscale activity in the metabolic balance of the Sargasso Se., Limnol. Oceanogr. 51, 2675–2689.

Moutin, T., Prieur, L., 2012. Influence of anticyclonic eddies on the Biogeochemistry from the Oligotrophic to the Ultraoligotrophic Mediterranean (BOUM cruise). Biogeosciences 9, 3827-3855. https://doi.org/ 10.5194/bg-9-3827-2012

Napolitano, E., Temel Oguz, T., Malanotte-Rizzoli, P., Yilmaz, Sansone, E., 2000. Simulations of biological production in the Rhodes and Ionian basins of the eastern Mediterranean. J. Mar. Syst. 24, 277-298.

Noskova, Y., Likhatskaya, G., Terentieva, N., Son, O., Tekutyeva, L., Balabanova, L., 2019. A Novel Alkaline Phosphatase/Phosphodiesterase, CamPhoD, from Marine Bacterium Cobetia amphilecti KMM 296. Mar. drugs 17, article 657. https://doi.org/10.3390/md17120657.

Oikonomou, A., Livanou, E., Mandalakis, M., Lagaria, A., Psarra, S., 2020. Grazing effect of flagellates on bacteria in response to phosphate addition in the oligotrophic Cretan Sea, NE Mediterranean. FEMS Microb. Ecol. 96, fiaa086. https://doi.org/10.1093/femsec/fiaa086

Pedrosa-Pàmies, R., Sanchez-Vidal, A., Canals, M., Lampadariou, N., Velaoras, D., Gogou, A., Parinos, C., Calafat, A., 2016. Enhanced carbon export to the abyssal depths driven by atmosphere dynamics, Geophys. Res. Lett. 43, 8626–863., https://doi.org/10.1002/2016GL069781.

Pitta, P., Nejstgaard, J. C., Tsagaraki, T. M., Zervoudaki, S., Egge, J. K., Frangoulis, C., Lagaria, A., Magiopoulos, I., Psarra, S., Sandaa, R.-A., Skjoldal, E. F., Tanaka, T., Thyrhaug, R., Thingstad, T. F., 2016. Confirming the "Rapid phosphorus transfer from microorganisms to mesozooplankton in the Eastern Mediterranean Sea" scenario through a mesocosm experiment. J. Pk. Res. 38, 502-52., https://doi.org/10.1093/plankt/fbw010

Popov, Y.I., 2004. Genesis and structure of the anticyclonic ierapetra zone in the levantine Basin. J Phys. Oceanogr. 14, 234-242.

Powley, H. T., Van Cappellen, P., Krom, M. D., 2017. Nutrient Cycling in the Mediterranean Sea: The Key to Understanding How the Unique Marine Ecosystem Functions and Responds to Anthropogenic Pressures. In: Mediterranean Identities - Environment, Society, Culture, edited by Furest-Bjelis B., Intech: 47-77

Prieur, L., D'Ortenzio, F., Taillandier, V., Testor, P., 2020. Physical oceanography of the Ligurian sea. In: The Mediterranean Sea in the era of global change (volume 1), evidence from 30 years of multidisciplinary study of the Ligurian sea, edited by Migon, C., Sciandra, A., Nival, P., ISTE Science Publications Ltd.: 49‑78 https://doi.org/10.1002/9781119706960.ch3

Pujo-Pay, M., Raimbault, P., 1994. Improvements of the wet-oxidation procedure for simultaneous determination of particulate organic nitrogen and phosphorus collected on filters. Mar. Ecol. Prog. Ser. 105, 203-207.

Pujo-Pay, M., Conan, P., Raimbault, P., 1997. Excretion of dissolved organic nitrogen by phytoplankton assessed by wet oxidation and N-15 tracer procedures. Mar. Ecol. Prog. Ser. 153, 99-111. https://doi.org/10.3354/meps153099.

Pujo-Pay, M., Conan, P., Oriol, L., Cornet-Barthaux, V., Falco, C., Ghiglione, J.-F., Goyet, C., Moutin, T., Prieur, L., 2011. Integrated survey of elemental stoichiometry (C, N, P) from the western to eastern Mediterranean Sea, Biogeosciences 8, 883–899. https://doi.org/10.5194/bg-8-883-2011

Pulido-Villena, E., Desboeufs, K. Djaoudi, K., Van Wambeke, F., Barrillon, S., Doglioli, A., Petrenko, A. Taillandier, V., Fu, F., Gaillard, T., Guasco, S., Nunige, S., Triquet, S., Guieu, C., 2021. Phosphorus cycling in the upper waters of the Mediterranean Sea (PEACETIME cruise): relative contribution of external and internal sources, Biogeosciences 18, 5871-7889. https://doi.org/10.5194/bg-18-5871-2021

Rahav, E., Herut, B., Spungin, D., Levi, A., Mulholland, M.R., Berman-Frank, I. 2021. Heterotrophic bacteria outcompete diazotrophs for orthophosphate in the Mediterranean Sea. Limnol. Oceanogr. 67, 159-171. https://doi.org/10.1002/lno.11983

Rahav, E., Paytan, A., Chien, C-T., Ovadia, G., Katz, T., Herut, B., 2016. The Impact of Atmospheric Dry Deposition Associated Microbes on the Southeastern Mediterranean Sea Surface Water following an Intense Dust Storm. Front. Mar. Sci. 3,127. https://doi.org/10.3389/fmars.2016.00127

Raimbault, P., Garcia, N., 2008. Evidence for efficient regenerated production and dinitrogen fixation in nitrogen-deficient waters of the South Pacific Ocean: impact on new and export production estimates. Biogeosciences 5, 323-338.

Ras, J., Claustre, H., Uitz, J., 2008. Spatial variability of phytoplankton pigment distributions in the Subtropical South Pacific Ocean: comparison between in situ and predicted data. Biogeosciences 5, 353–369. https://doi.org/10.5194/bg-5-353-2008

Reich, T., Ben-Ezra, T., Belkin, N., Aharonovich, D., Roth-Rosenberg, D., Givati, S., Bialik, M., Herut, B., Berman-Frank, I., Frada, M., Krom, M., D., Lehahn, Y., Rahav, E., Sherr, D., 2022. A year in the life of the Eastern Mediterranean: Monthly dynamics of phytoplankton and bacterioplankton in an ultra-oligotrophic sea. Deep-Sea Res. part I 182, article 103720. https://doi.org/10.1016/j.dsr.2022.103720

Rosenberg, H., Gerdes, R. G., and Chegwidden, K., 1977. Two systems for the uptake of phosphate in *Escherichia coli*. J. Bacteriol. 131, 505–511.

Sala, M. M., Karner, M., Arin, L., Marrassé, C., 2001. Measurement of ectoenzyme activities as an indication of inorganic nutrient imbalance in microbial communities. Aquat. Microb. Ecol. 23, 301-311.

Salihoglu, B., Saydam, C., Basturk, Ö., Yilmaz, K., Goçmen D., Hatipoglu, E. Yilmaz, A., 1990. Transport and Distribution of Nutrients and Chlorophyll-a by Mesoscale Eddies in the Northeastern Mediterranean. Mar. Chem. 29, 375-390.

Sato, M., Sakuraba, R., Hashihama, F., 2013. Phosphate monoesterase and diesterase activities in the North and South Pacific Ocean. Biogeosciences 10, 7677–7688. https://doi.org/10.5194/bg-10-7677-2013

Smith, D. C., Azam, F., 1992. A simple, economical method for measuring bacterial protein synthesis rates in sea water using 3H-Leucine, Mar. Microb. Food Webs 6, 107-114.

Steemann Nielsen, E., 1952. The use of radioactive carbon (14C) for measuring organic production in the sea. Journal du Conseil Permanent International pour l'Exploration de la Mer, 18, 117–140.

Su, B., Song, X., Duhamel, S., Mahaffey, C., Davis, C., Ivančić, I., Liu, J., 2023. A data set of global ocean alkaline phosphatase activity. Sci. data 10, 205. https://doi.org/10.1038/s41597-023-02081-7

Suzuki, S., Ferjani, A., Suzuki, I., and Murata, N., 2004. The SphS-SphR Two Component System is the exclusive sensor for the induction of gene expression in response to phosphate limitation in *Synechocystis*. J. Biol. Chem. 279, 13234–13240. https://doi.org/10.1074/jbc.M313358200

Sweeney, E. N., McGillicuddy Jr, D. J., Buesseler, K. O., 2003. Biogeochemical impacts due to mesoscale eddy activity in the Sargasso Sea as measured at the Bermuda Atlantic Time-series Study (BATS). deep Sea Res. Part II 50, 3017-3039. https://doi.org/10.1016/j.dsr2.2003.07.008

Taillandier, V., D'Ortenzio, F., Prieur, L., Conan, P., Coppola, C., Cornec, M., Dumas, F., Durrieu de Madron, X., Fach, B., Fourrier, M., Gentil, M., Hayes, D., Husrevoglu, H., Legoff, H., Le Ster, L., Örek, H., Ozer, T., Poulain, P.M., Pujo-Pay, M., Ribera d'Alcalà, M., Salihoglu, B., Testor, P., Velaoras, D., Wagener, T., Wimart-Rousseau, C., 2022. Sources of the Levantine Intermediate Water in Winter 2019. J. Geophys. Res. Oceans 27, e2021JC017506. https://doi.org/10.1029/2021JC017506.

Taillandier, V., Prieur, L., D'Ortenzio, F., Ribera d'Alcalà, M., Pulido-Villena, E., 2020. Profiling float observation of thermohaline staircases in the western Mediterranean Sea and impact on nutrient fluxes, Biogeosciences 17, 3343-3366, https://doi.org/10.5194/bg-17-3343-2020

Tanaka, T., Henriksen, P., Lignell, R., Olli, K., Seppala, J., Tamminen, T., Thingstad, F., 2006. Specific affinity for phosphate uptake and specific alkaline phosphatase activity as diagnostic tools for detecting phosphorus-limited phytoplankton and bacteria. Estuaries Coast. 29, 1-16. https://doi.org/10.1007/BF02781823

Tanaka, T., Thingstad, T. F., Christaki, U., Colombet, J., Cornet-Barthaux, V., Courties, C., Grattepanche, J.-D., Lagaria, A., Nedoma, J., Oriol, L., Psarra, S., Pujo-Pay, M., and Van Wambeke, F., 2011. Lack of P-limitation of phytoplankton and heterotrophic prokaryotes in surface waters of three anticyclonic eddies in the stratified Mediterranean Sea, Biogeosciences 8, 525–538. https://doi.org/10.5194/bg-8-525-2011

Thingstad, T. F., Krom, M. D., Mantoura, R. F., Flaten, G. A., Groom, S., Herut, B., Kress, N., Law, C. S., Pasternak, A., Pitta, P., Psarra, S., Rassoulzadegan, F., Tanaka, T., Tselepides, A., Wassmann, P., Woodward, E. M., Wexels Riser, C., Zodiatis, G., Zohary, T., 2005. Nature of Phosphorus Limitation in the Ultra-oligotrophic Eastern Mediterranean, Science 309, 1068–1071. https://doi.org/10.1126/science.1112632

Thomson, B., Wenley, J., Lockwood, S., Twigg, I., Currie, K., Herndl, G., Hepburn, C. D., Baltar, F., 2020. Relative Importance of Phosphodiesterase vs. Phosphomonoesterase (Alkaline Phosphatase) Activities for Dissolved Organic Phosphorus Hydrolysis in Epi and Mesopelagic Waters. Front. Earth Sci. 8, article 560893. https://doi.org/10.3389/feart.2020.560893

Van Mooy, B. A., Fredricks, H. F., Pedler, B. E., Dyhrman, S. T., Karl, D. M., Koblicek, M., Lomas, M. W., Mincer, T. J., Moore, L. R., Moutin, T. Rappé, M. S., Webb, E.A., 2009. Phytoplankton in the ocean use non-phosphorus lipids in response to phosphorus scarcity. Nature 458, 69-72.

Van Wambeke, F., Christaki, U., Giannakourou, A., Moutin, T., Souvemerzoglou, K., 2002. Longitudinal and vertical trends of bacterial limitation by phosphorus and carbon in the Mediterranean Sea. Microb. Ecol. 43, 119-133. https://doi.org/10.1007/s00248-001-0038-4

Van Wambeke, F., Conan, P., Pujo-Pay, M., Taillandier, V., Crispi, O., Pavlidou, A., Nunige, S., Didry, M., Salmeron, C., Pulido-Villena E., 2024. Phosphomonoesterase and phosphodiesterase activities in the eastern Mediterranean during two contrasted seasonal situations, Biogeosciences 21, 2621–2640, https://doi.org/10.5194/bg-21-2621-2024

Van Wambeke, F., Taillandier, V., Desboeufs, K., Pulido-Villena, E., Dinasquet, J., Engel, A., Marañón, E., Ridame, C., Guieu, C., 2021. Influence of atmospheric deposition on biogeochemical cycles in an oligotrophic ocean system. Biogeosciences 15, 5699–5717. https://doi.org/10.5194/bg-18-5699-2021

Varkitzi, I., Psarra, S., G., A., Pavlidou, A., Krasakopoulou, E., Velaoras, D., Papathanassiou, E., Pagou, K., 2020. Phytoplankton dynamics and bloom formation in the oligotrophic Eastern Mediterranean: Field studies in the Aegean, Levantine and Ionian seas. Deep-Sea Res. Part II 171, article 104662. https://doi.org/10.1016/j.dsr2.2019.104662

Velaoras, D., Papadopoulos, V.P., Kontoyiannis, H., Cardin, V., Civitarese, G., 2019. Water masses and hydrography during April and June 2016 in the Cretan Sea and Cretan Passage (Eastern Mediterranean Sea). Deep Sea Res. Part II 164, 25-40. https://doi.org/10.1016/j.dsr2.2018.09.005

Vidussi, F., Claustre, H., Manca, B., Luchetta, A., Marty, J-C., 2001. Phytoplankton pigment distribution in relation to upper thermocline circulation in the eastern Mediterranean Sea during winter. J. Geophys. Res. 106, 19939-19956.

Yamaguchi, H., Arisake, H., Otsuka, N. Tomaru, Y., 2014. Utilization of phosphate diesters by phosphodiesterase-producing marine diatoms. J. Pk. Res. 36, 281-285. https://doi.org/10.1093/plankt/fbt091

Yamaguchi, T., Sato, M., Hashihama, F., Ehama, M., Shiozaki, T., Takahashi, K., Furuya, K., 2019. Basin-Scale Variations in Labile Dissolved Phosphoric Monoesters and Diesters in the Central North Pacific Ocean. Journal of Geophysical Research: Oceans 124, 3058–3072. https://doi.org/10.1029/2018JC014763

Yılmaz, A., Tugrul, S., 1998. The effect of cold- and warm-core eddies on the distribution and stoichiometry of dissolved nutrients in the northeastern Mediterranean. J Mar. Syst. 16, 253–268.

Zaccone, R., Boldrin, A., Caruso, G., La Ferla, R., Maimone, G., Santinelli, C., Turchetto, M., 2012. Enzymatic Activities and Prokaryotic Abundance in Relation to Organic Matter along a West–East Mediterranean Transect (TRANSMED Cruise). Microb. Ecol. 64, 54-66. https://doi.org/10.1007/s00248-012-0011-4

Zhang, J.-Z., Chi, J., 2002. Automated analysis of nano-molar concentrations of phosphate in natural waters with liquid waveguide, Environ. Sci. Technol. 36, 1048-1053, https://doi.org/10.1021/es011094v

Zodiatis, G., Brenner, S., Gertman, I., Ozer, T., Simoncelli, S., Ioannou, M., Savva, S., 2023. Twenty years of in-situ monitoring in the south-eastern Mediterranean Levantine basin: Basic elements of the thermohaline structure and of the mesoscale circulation during 1995-2015. Front. Mar. Sci. 9, article 1074504. https://doi.org/10.3389/fmars.2022.1074504

Zohary, T., Herut, B., Krom, M. D., Mantoura, R. F., Pitta, P., Psarra, S., Raap, A. K., Rassoulzadegan, F., Strambler, N., Tanaka, T., Thingstad, F., Woodward, E., 2005. P-limited bacteria but N and P colimited phytoplankton in the Eastern Mediterranean. A microcosm experiment. Deep Sea Res. Part II 52, 3011-3023. https://doi.org/10.1016/j.dsr2.2005.08.011

Table 1. List of PERLE 1 and PERLE 2 stations. Group category, coordinates, depth of mixed layer (MLD) depth of phosphacline (ZPcline) and nitracline (ZNcline) with their associated standard errors.Those 2 stations have missing data (hprok abundance for st 58, L_{DOP} for st 16) and were not included in the PCA, for statistics they were included in groups *a posteriori*, thanks to their non-missing biogeochemical characteristics. ** Some statistics: mean standard error and % variation for both cruises, ratio of means (P2:P1) and p value for statistical difference between the 2 cruises (Mann-Whiney test).

			date	°N	°E	m	m	m
cruise	group	st	d/m/y	Lat	Long	MLD	ZPcline	ZNcline
PERLE1	A	2	10/10/2018	34.82	26.52	38	106 ± 42	126 ± 18
PERLE1	A	5	11/10/2018	34.29	26.51	48	188 ± 77	154 ± 20
PERLE1	A	12	12/10/2018	33.32	26.49	22	119 ± 10	105 ± 5
PERLE1	A	15	15/10/2018	34.21	25.95	30	145 ± 34	123 ± 56
PERLE1	A*	16	15/10/2018	34.21	25.65	25	193 ± 8	143 ± 3
PERLE1	A	19	16/10/2018	34.21	26.76	23	175 ± 73	137 ± 47
PERLE1	A	20	16/10/2018	34.21	27.1	36	122 ± 24	90 ± 17
PERLE1	A	23	16/10/2018	33.9	26.64	35	167 ± 33	123 ± 8
PERLE1	A	25	18/10/2018	34.21	26.05	88	239 (n=2)	185 ± 17
PERLE1	A	27	19/10/2018	33.83	27.09	19	100 ± 10	83 ± 30
PERLE1	A	30	20/10/2018	33.82	27.82	18	135 ± 11	98 ± 14
PERLE2	F	1	27/02/2019	35.86	25.3	145	82 ± 25	60 ± 46
PERLE2	F	13	28/02/2019	35.62	23.54	118	247 ± 59	188 ± 87
PERLE2	F	15	01/03/2019	35.95	23.76	269	164 ± 19	90 ± 65
PERLE2	C	21	02/03/2019	34.44	22.82	27	115 ± 144	109 ± 59
PERLE2	C	26	02/03/2019	34.44	23.73	113	94 ± 14	70 ± 19
PERLE2	C	35	04/03/2019	34.33	24.52	53	164 ± 48	144 ± 29
PERLE2	C	44	05/03/2019	33.62	24.38	61	67 ± 12	24 ± 8
PERLE2	B	50	06/03/2019	34.32	25.3	213	258 ± 39	211 ± 62
PERLE2	D*	58	07/03/2019	34.29	26.09	97	151 ± 31	101 ± 26
PERLE2	E	68	08/03/2019	33.59	28.81	34	89 ± 6	40 ± 30
PERLE2	C	75	10/03/2019	33.86	27.99	45	73 ± 6	89 ± 48
PERLE2	E	80	10/03/2019	33.96	27.32	14	37 ± 9	0 ± 9
PERLE2	E	90	12/03/2019	34.68	26.9	25	82 ± 7	64 ± 5
PERLE2	E	94	12/03/2019	34.94	26.74	19	15 ± 3	0 ± 1
PERLE2	B	104	13/03/2019	35.37	26.66	63	177 ± 34	134 ± 30
PERLE2	B	108	13/03/2019	35.84	27.43	103	265 (n=2)	240 (n=2)
PERLE2	D	111	14/03/2019	33.96	27.32	53	45 ± 9	32 ± 5
PERLE2	D	116	15/03/2019	34.68	26.9	48	104 ± 31	85 ± 2
				P1**	mean	35	154	124
					sd	20	43	30
					% var	57	28	24
				P2	mean	83	124	93
					sd	69	76	69
					% var	83	61	74
					Ratio P2:P1	2.40	1	1
					P diff	0.015	ns	ns

Table 2. List of PERLE 1 and PERLE 2 stations. Group category; integrated stocks (0-200 m depth) for nitrate+nitrite (I NOx), inorganic phosphate (I DIP), Labile DOP (I L_{DOP}) and dissolved organic phosphorus (DOP); integrated Total chlorophyll a stocks (I Tchla); integrated bacterial production (IBP, in the 0-200m layer ** Some statistics: mean standard error and % variation for both cruises, ratio of means (P2:P1) and p value for statistical difference between the 2 cruises (Mann-Whiney test).

			mmol m^{-2}	mmol m^{-2}	mmol m^{-2}	mmol m^{-2}	mg m^{-2}	mg C m^{-2} d^{-1}
cruise	group	st	I NOx	I DIP	I L_{DOP}	I DOP	ITchla	IBP
PERLE1	A	2	95	4.8	0.98	4.1	16.1	na
PERLE1	A	5	55	2.6	1.28	7.6	14.6	na
PERLE1	A	12	128	3.7	1.24	3.5	13.4	na
PERLE1	A	15	109	3.2	0.96	4.8	13.1	na
PERLE1	A*	16	61	2.4	nd	5.6	11	na
PERLE1	A	19	96	3.5	0.73	5.3	21.4	na
PERLE1	A	20	157	3.8	1.05	6.3	15	na
PERLE1	A	23	61	3	1.05	9.9	23.8	na
PERLE1	A	25	19	2	0.63	4.9	20.9	na
PERLE1	A	27	156	4.5	1.33	5.4	16.5	na
PERLE1	A	30	128	3.4	0.79	1.8	16.8	na
PERLE2	F	1	221	5.9	5.9	15.2	51.7	28
PERLE2	F	13	247	4.5	8.08	13.7	59.2	31.2
PERLE2	F	15	226	4.8	2.3	15.2	66.2	29.7
PERLE2	C	21	330	7.5	1.09	8.1	33.2	22.6
PERLE2	C	26	276	6.6	1.6	10.1	39.8	29.9
PERLE2	C	35	158	3	1.7	11.6	52.6	39.3
PERLE2	C	44	340	8	2.43	10.3	28.2	19.3
PERLE2	B	50	99	1.7	1.75	13.8	69.3	31.2
PERLE2	D*	58	314	5.7	2.34	9.3	60.9	43.7
PERLE2	E	68	463	12.3	1.93	9.1	40.3	30.1
PERLE2	C	75	265	4.9	3.4	11.9	48.1	26.6
PERLE2	E	80	520	14.7	1.9	8.1	65.6	55.4
PERLE2	E	90	389	10.3	3.17	11.5	45.6	55.2
PERLE2	E	94	753	24.7	2.72	8.2	26.5	26.5
PERLE2	B	104	152	2.7	3.05	5.8	39.5	39
PERLE2	B	108	113	1.7	2.88	4.5	67.4	39.9
PERLE2	D	111	470	13.2	2.73	7.7	63.8	77.6
PERLE2	D	116	426	12.3	2.23	8	38.9	49.5
	P1**	mean	97	3.3	1.01	5.4	16.6	
		sd	44	0.9	0.24	2.1	3.9	
		% var	46	26	24	39	24	
	P2	mean	320	8	2.84	10.1	50	37.5
		sd	165	5.8	1.67	3.1	14	14.5
		% var	52	72	59	30	28	39
		Ratio P2:P1	3.31	2.4	2.83	1.88	3.01	
		P diff	<0.001	0.006	<0.001	< 0.001	< 0.001	

Table 3 Integrated heterotrophic bacterial production rates (BPI, 0-100m, PERLE2 cruise only) and primary production (PPI) during PERLE1 and PERLE2 cruises. Bacterial carbon demand (BCD) was calculated assuming a bacterial growth efficiency (BGE) of 10 %, with BCD=BP/BGE. For PERLE1, the CTDs sampled for PP were at the same place and days that the CTDs used for measuring ectoenzymatic activities, DOP stocks and nutrients (under parenthesis).*ctd 83 was sampled just for BP and PP and not ectoenzymatic activities and DOP pools, but has other characteristics close to the stations of the E group.

cruise	ctd number for BP, enzymes	group	mgC m^{-2} d^{-1} BPI	ctd number for PP	mg C m^{-2} d^{-1} PPI	BP/PP ratio	BCD/PP ratio
PERLE1	(2)	A		3	39		
PERLE1	(15)	A		14	95		
PERLE1	(25)	A		24	123		
PERLE1	(27)	A		26	123		
PERLE2	1	F	17.8				
PERLE2	13	F	18.2				
PERLE2	15	F	15.2	15	360	0.042	0.42
PERLE2	21	C	15.6				
PERLE2	26	C	24.5				
PERLE2	35	C	24.7	35	413	0.060	0.60
PERLE2	44	C	17.2				
PERLE2	50	B	14.7				
PERLE2	58	D	27.9				
PERLE2	68	E	27.4				
PERLE2	75	C	18.6	75	405	0.046	0.46
PERLE2	80	E	46.3				
PERLE2	83	E*	24.9	83	411	0.061	0.61
PERLE2	90	E	46.7	90	509	0.092	0.92
PERLE2	94	E	20.4				
PERLE2	104	B	27.6				
PERLE2	108	B	24.1				
PERLE2	111	D	65.9				
PERLE2	116	D	39.3	116	364	0.108	1.08

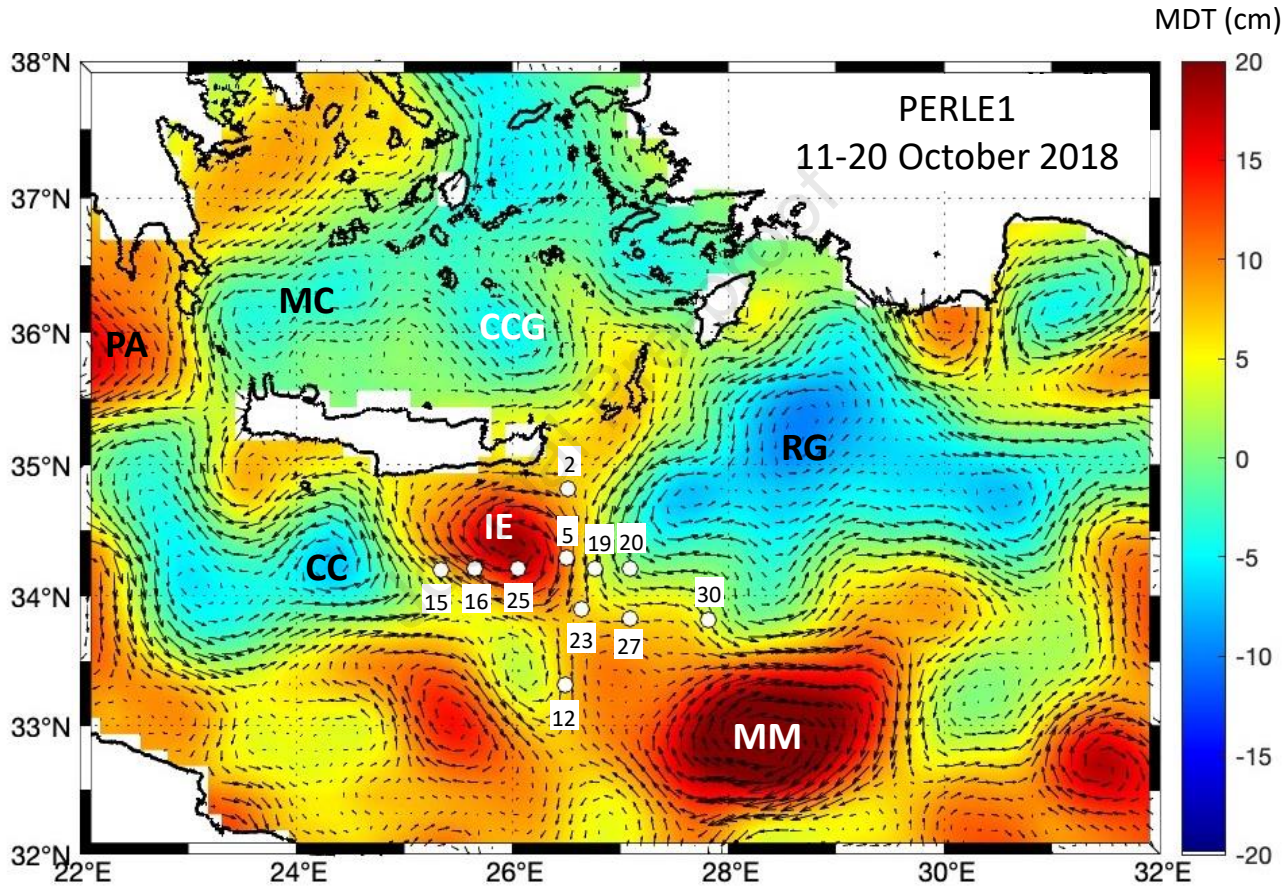
MDT (cm)
PERLE1
11-20 October 2018
MC
CCG
PA
RG
IE
CC
MM
2
5
19
20
15
16
25
30
23
27
12
38°N
37°N
36°N
35°N
34°N
33°N
32°N
22°E
24°E
26°E
28°E
30°E
32°E
20
15
10
5
0
-5
-10
-15
-20

Fig. 1

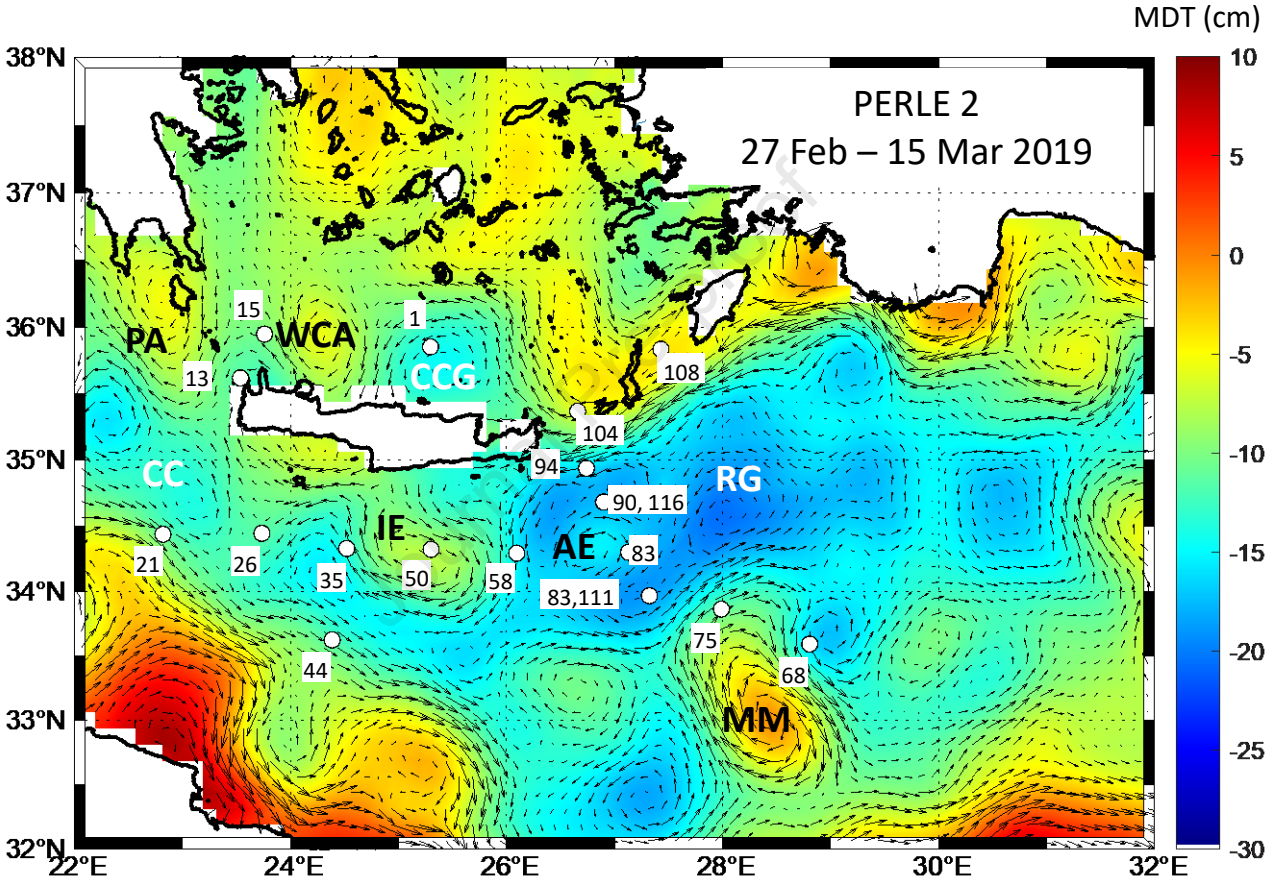
MDT (cm)
PERLE 2
27 Feb – 15 Mar 2019
38°N
37°N
36°N
35°N
34°N
33°N
32°N
22°E
24°E
26°E
28°E
30°E
32°E
10
5
0
-5
-10
-15
-20
-25
-30
PA
WCA
CCG
CC
IE
AE
RG
MM
15
1
13
108
104
94
90, 116
83
83,111
21
26
35
50
58
75
68
44

Fig. 2

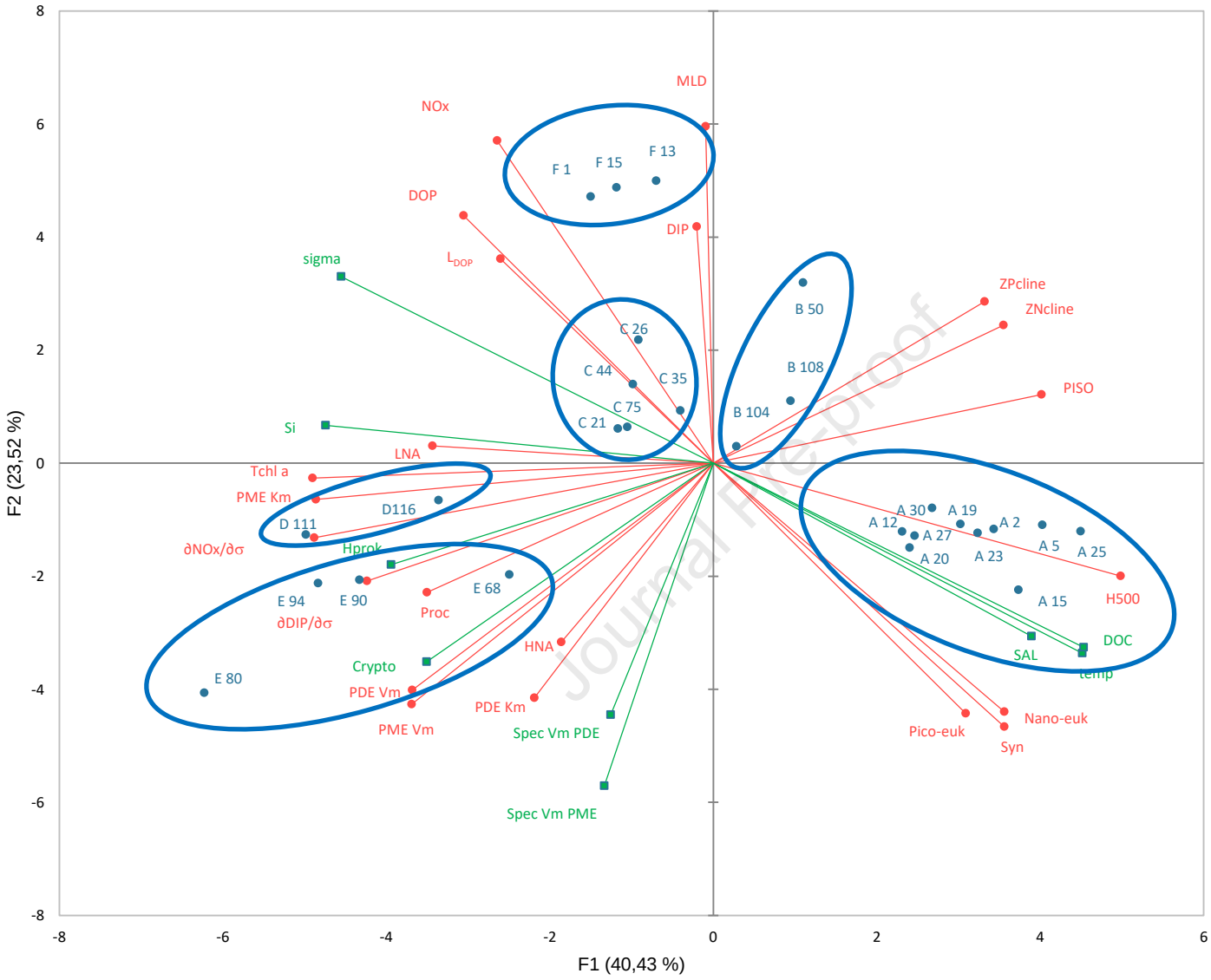

Fig. 3

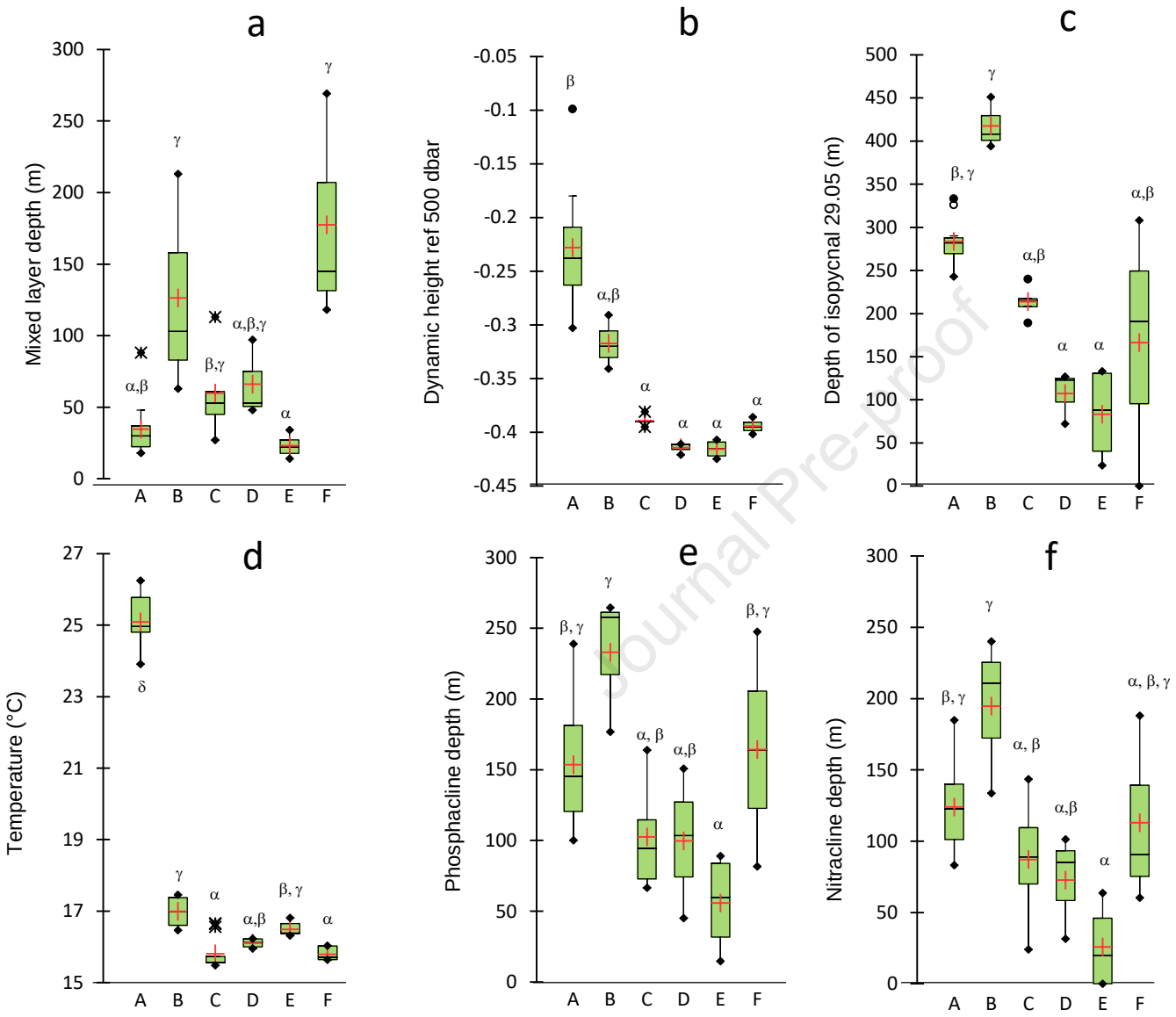

Fig. 4

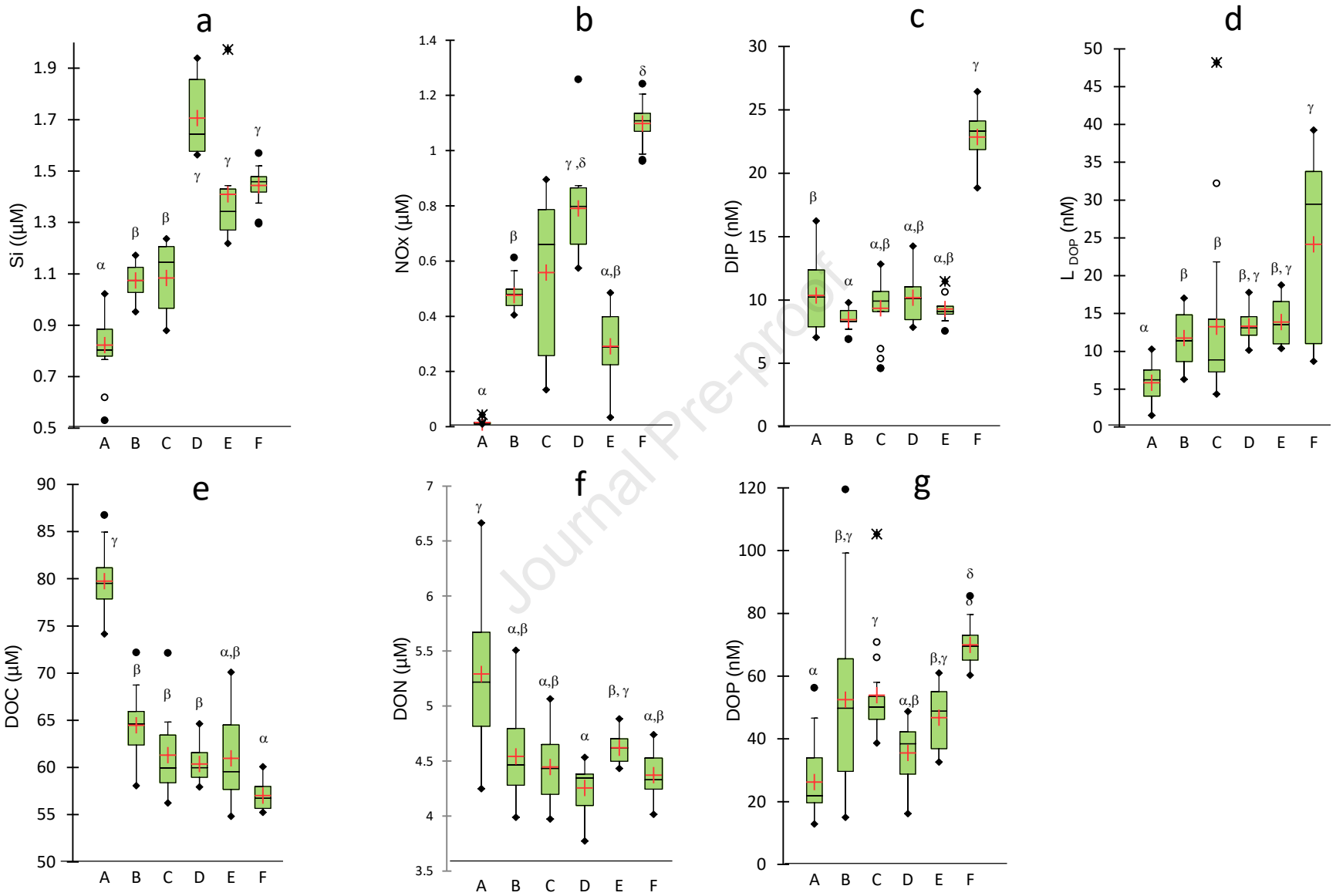

Fig. 5

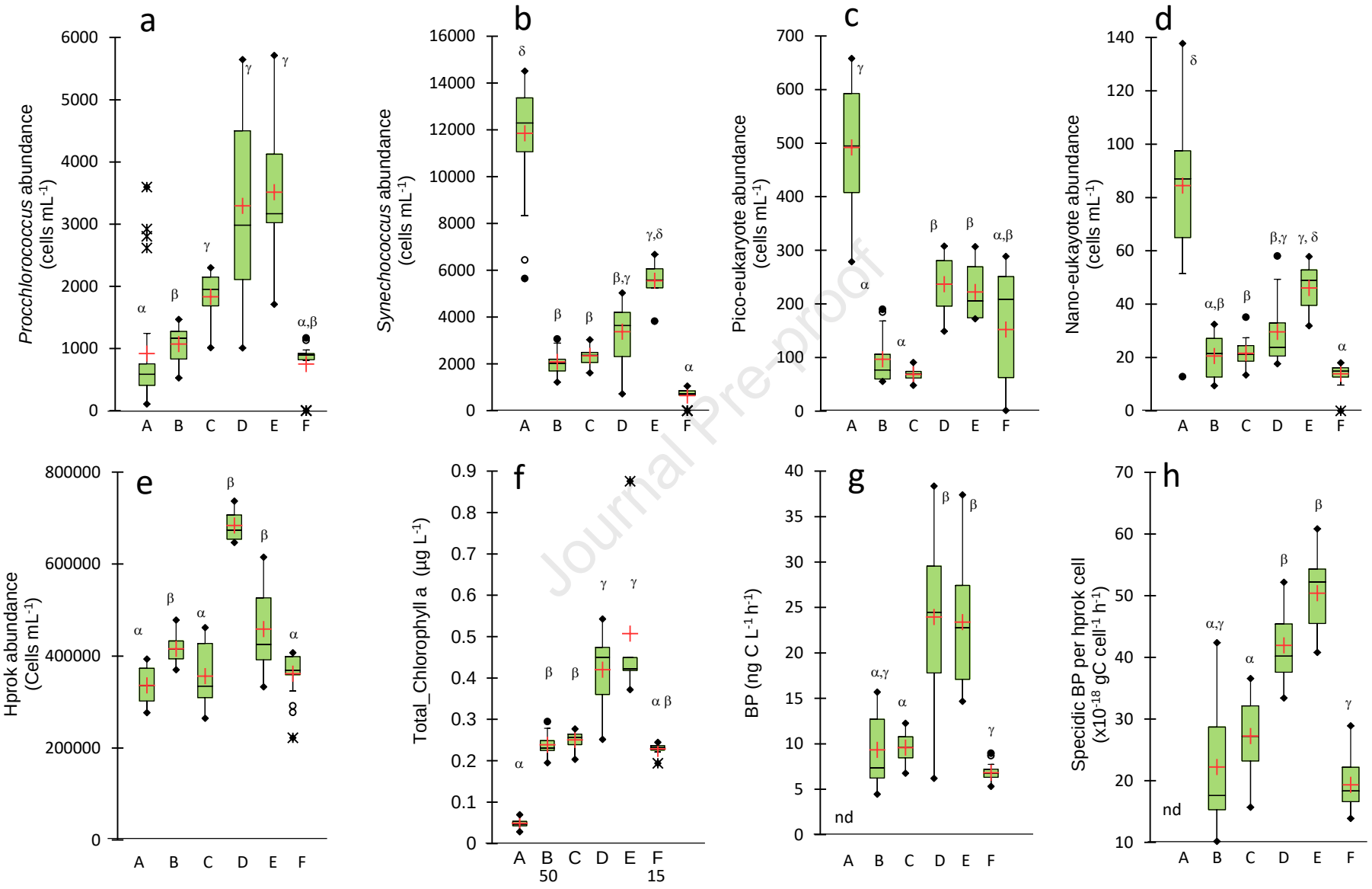

Fig. 6

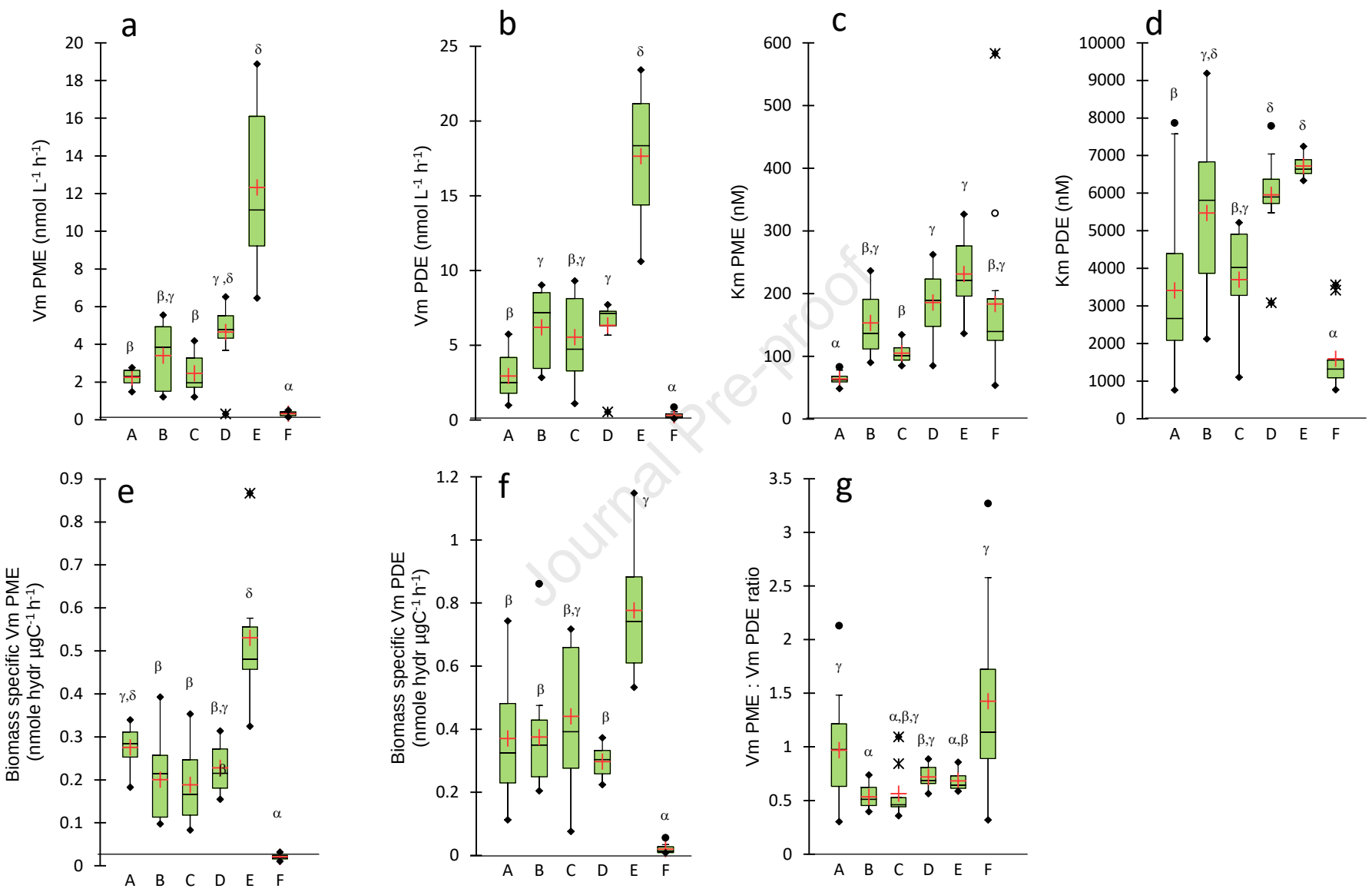

Fig. 7

Declaration of interests

☒ The authors declare that they have no known competing financial interests or personal relationships that could have appeared to influence the work reported in this paper.

☐ The authors declare the following financial interests/personal relationships which may be considered as potential competing interests: